The golden roof of the Shwedagon Pagoda

Improving metal-organic interfacial adhesion: how can we provide a high adhesion strength in a system that contains metals with unassociated chemical properties?

Lise Vermeersch

Master thesis submitted under the supervision of
Prof. dr. ir. Tom Hauffman

The co-supervision of
Prof. dr. ir. Herman Terryn
dr. ir. Vanina Cristuado

In order to be awarded the Master's Degree in
Master of Science in Chemical and Materials engineering

Academic year
2020-2021

Abstract

Improving metal-organic interfacial adhesion: how can we provide a high adhesion strength in a system that contains metals with unassociated chemical properties? (Lise Vermeersch, 2020-2021)

Master of Science in Chemicals and Materials Engineering: Profile Materials

The Shwedagon Pagoda is the largest golden temple in the world and a very important pilgrimage site for the Buddhist community in Myanmar. The roof of this temple, however, faces delamination issues demanding for an expensive restoration each five years. The gold on the roof panels, consisting of a layered copper-glue-gold structure, is not durably attached to the underlying surface. This issue introduces the interesting topic of adhesion of organic materials on metals that have unassociated chemical properties on the surface. The goal of this thesis is to analyze this difference in chemical interaction between metals and organic material using the gold, a noble material, and the copper, a material that contains a native oxide layer, as examples. The chemical interaction with different adhesives will be mimicked using model molecules and the organo-metallic interface will be characterized using X-ray photo-electron spectroscopy (XPS). High resolution spectra allow to decompose the contributions to the XPS peaks and learn more about the species present in and on the surface by analyzing components present at the interface, as well as the relative ratio of their constituting atoms. Both copper and gold will first be analyzed as bare substrates and then subsequently submerged in diethylenetriamine (DETA, containing amine species as present in the currently used glue), succinic acid (SA, containing carboxylic acid as present in historically used natural oils) and thiolic solutions (as thiols were shown to interact with both gold and copper). It was found that these compounds interact very differently with the noble gold metal, compared to the native oxide layer of copper. Where DETA and SA show a good interaction with the copper surface, they interact poorly with the gold surface. Thiolic compounds interact well with both copper and gold, but the thiols require some time to self-assemble onto the gold (24h). Finally, the copper was oxidized to analyze the different interactions with thiolic solutions. CuO species interacted better with the thiols than bare copper or Cu_2O species. This allowed to indicate a fundamental difference in chemical interaction of noble metals and metals that contain a native oxide layer and propose possible improvement routes for the gluing of gold on the temple in Myanmar.

Keywords: Gold surface, copper surface, organ-metallic interaction, interfacial adhesion, X-ray electron spectroscopy, Shwedagon Pagoda

Acknowledgement

Throughout writing the writing and preparation of this manuscript I have received a great deal of support and assistance.

I would like to thank my promotor Professor Tom Hauffman for his support and guidance all throughout this project. Your insightful comments and ideas have taught me to approach issues in a way a researcher would. This is a skill I will cherish and use throughout my further career.

I would like to thank my supervisor Professor Herman Terryn for his guidance and for giving me the opportunity to work on this interesting multidisciplinary project by contacting the officials in Myanmar. Your experience and insights truly brought this thesis to another level.

I would like to thank my supervisor Doctor Vanina Cristuado for her guidance and never ceasing work ethic. You taught me the degree of precision required to successfully research and helped me at each step of the way.

I would like to thank Kitty Baert for her work in acquiring all the XPS spectra and for sharing her insights, expertise and knowledge in this technique.

I would also like to thank Priya Laha and Thomas Collet for their insights on this thesis.

And finally, a thank you to my family, friends and especially my boyfriend, for their love and support. Your encouragement enables me to work a bit harder each and every day.

List of abbreviations

XPS	X-ray photo-electron spectroscopy
XRD	X-ray diffraction
DFT	Density functional theory
DETA	Diethylenetriamine
THF	Tetrahydrofuran
SEM	Scanning electron microscopy
EDX	Energy dispersive X-ray analysis
CPS	Counts per second
FWHM	Full width at half maximum
BE	Binding energy
SA	Succinic acid

Content

1. Introduction

1.1. The Shwedagon Pagoda

The Shwedagon Pagoda (Figure 1) is one of the most important Buddhist pilgrimage sites in the world. [1] It is situated on the Singattura Hill, in Yangon, the former capital of Burma or Myanmar. It has been the background of the many political battles the country has known, ranging from the colonization by Great Britain to the military coup in 1962 that still affects the country today. It was the pagoda where students protested the elites' "University Act", where general Aung San demanded independence from Great Britain and where his daughter Aung San Suu Kyi demanded the military reign to end twenty years later. [2]

Figure 1: A picture of the Shwedagon Pagoda in Yangun, Myanmar. [1]

The pagoda appears to be the combination of a typical pagoda, as seen in many Buddhist structures throughout Asia, and a stupa, which is a bell-shaped, enclosed structure that includes relics. The stupa of this temple is entirely covered in gold, accounting for a total of 20.000 kilograms. The gold mainly comes from gifts of visitors, a custom that originated when Queen Shin Sawbu donated her weight in gold to the temple in the 15th century.[2]

1.2. The golden roof

The applied gold is rolled next to the site and glued to copper plates using a glue provided by Huntsman. The preliminary surface treatment is unknown. After about five years about 10.000 to 100.000 gold plates start to delaminate, and the structure must be restored. When the gold needs to be replaced, scaffolds are mounted, and the gold is removed by hand, demanding an investment of about 20 million euros.[3] The gold is remolten in a small factory next to the temple, which allows to reuse the precious material and only replace the plates that cannot be recovered.

Figure 2: Left: gluing of the gold plates onto the copper next to the Shwedagon Pagoda, Right: delamination of the gold from the copper plates.

The durability of the applied gold onto the structure has been a problem for many years. First a local glue was used, but the gold seemed to delaminate rapidly. Therefore, three different application procedures were used in an attempt find one that is durable. At a certain location the gold is fire-gilded, at another it is electroplated and at yet another one it is glued onto copper plates. This thesis will focus on the adhesion by gluing. This work will explore chemical interactions between the metals and adhesives in an attempt to propose possible improvement routes.

Subsequently to a workshop on gold gilding in Yangon (October 2019), a collaboration with the Technological University of Yangon was organized by Herman Terryn (VUB) in order to investigate the delamination process of the gold glued and the copper. It is important to note that the collaboration with Myanmar partners during this thesis was impaired due to the military coup that emerged in Myanmar.

2. Problem statement

The analyzed roof panels consist of three elements: copper plates, epoxy-based glue with amine components and relatively thick (100 µm) rolled gold plates. It is this thickness of the gold plates that is extraordinary in the world of cultural heritage, as statues and buildings are normally gilded with gold leaf. In most cultural heritage, gold leaf is glued with natural oils and must be restored each 25-30 years.[4] Due to the excess of gold in Myanmar and the large number of gifts of visitors, however, the monument is covered with much thicker plates. Up until this point, there is no scientific explanation for the different lifetimes of these systems.

The glue that is currently used is purchased at Huntsman and is based on epoxy with a hardener based on amines. The glue is prepared in a small factory next to the site, where the pure gold plates are rolled as well. It is applied by hand, as can be seen in Figure 2.

There are many possible reasons for the delamination of the gold plates, like the thermal expansion difference between the glue and the metals or corrosion of the copper metal, which can all be led back to the inherent strength of the bond formed between the metals and the glue. **Therefore, the focus of this thesis will be the chemical interfacial adhesion of organic-metal systems that contain both noble and oxidized metal surfaces.** The challenge will be to find an organic molecule that interacts strongly with both the noble gold metal and the sometimes complex and naturally formed copper oxides.

3. State of the art

3.1. Adhesion of organic components on gold and copper substrates

3.1.1. Surface interactions

The adhesion of organic components to metals is widely studied as an important characteristic of the coating of metal substrates.[5] To protect the underlying metal from corrosion, next to the barrier properties of the coating itself, the adhesion between the organic material and the metal(oxide) is crucial for proper preservation of the metal properties. Since different metals react differently to the atmosphere and can therefore have varying properties at the surface, it is of course impossible to investigate all possible combinations of metals and organic materials and not all combinations are already described in literature.

The interactions of a metal or metal oxide with organic material can be either physical or chemical (Table 1). The so-called primary or chemical interactions occur when electron exchange occurs between the atoms. This can be in the form of an ionic bond, a covalent bond, or an acid-base

interaction (Lewis or Brönsted). These interactions are very strong, but short range. This makes the topography of the substrate an important factor for chemical bond formation, as it will influence the wetting of the material and thus the proximity of both the substrate and the organic material.

Table 1: Bond type, strength hand equilibrium length for different types of interactions.[6]

Bond type	Bond energy (kJ/mol)	Equilibrium length (nm)
Primary, chemical		
Ionic	600-1000	0.2-0.4
Covalent, Bronsted	60-800	0.1-0.3
Metallic	100-350	0.2-0.6
Acid-base interactions		
Conventional Bronsted	<1000	
Lewis	<80	
Secondary, physical		
Hydrogen	50	0.3
Van der Waals		
London, dispersion	1-40	<1
Keesom orientation	2-8	0.4
Debye induction	<2	0.4

The Van Der Waals interactions are the so-called secondary or physical interactions, which don't include an electron transfer. Van Der Waals forces consist of three sorts of interactions: Debye, Keesom and London forces. Debye (induced dipoles) and Keesom (permanent dipoles) are polar forces and occur between polarizable and polarized molecules. London forces are forces that depend on the motion of the electron cloud, regardless of the dipoles of the molecule. Besides this, hydrogen bonding can occur between a hydrogen atom and an electronegative atom, because of the difference in electronegativity. These interactions are weak, but long range, making that the combination of a large number of these interactions can form a strong connection between two materials.[7]

As polymer-metal adhesion is such a difficult mechanism to describe, there are seven accepted theories that describe polymer adhesion, being mechanical interlocking, electrostatic interactions, diffusion, wettability, chemical bonding, weak boundary layer interactions and acid-base interactions.[8] For a long time, it was believed that a strong bond formation between metals and organic material or polymers was governed by the roughness of the substrate, because it increased the surface area available for mechanical interlocking. Watts et al. refuted this statement and attributed the adhesion strength to an increase in material surface available for bond formation. Therefore, this thesis will focus on the chemical bond formation on metallic substrates and will thus focus on the latter three theories.[9]

3.1.2. Influence of the surface state of the metal

The surface of different metals will, because of their crystal structure, contain atoms with different coordination numbers. Atoms like oxygen and sulfur, that tend to bind strongly to the surface, prefer a very symmetrical lattice, since their coordination with the lattice will be the highest here. Larger molecules have more modes of orientation and will therefore be able to form bonds with many different types of lattices.[10]

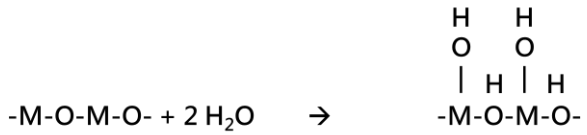

Figure 3: Schematic representation of the reaction of metal oxides with water [11]

The surface of a metal oxide contains a metal cation and an oxygen anion. This makes the surface polar and thus more susceptible to some chemical reactions. An example is the reaction of metals with water to form hydroxides, as shown in Figure 3.[11] For other reactions, like the interaction of copper with sulfur atoms as found in thiols, the presence of oxides will decrease the possibility of bond formation, as the interaction will occur between the molecule and the copper atom, rather than with the hydroxyl group. As the copper present in the oxide will have a lower electron density, it will thus be less prone to interact with a sulfur atom.[12]

3.1.3. Pretreatments and their importance

Polymers used as adhesives are known to have a low surface free energy and a limited number of polar groups, and are therefore not very susceptible to chemical bond formation on metal surfaces.[13] Therefore, some adjustments to either the polymer or the metal should be made to improve the adhesion strength.[14] These adjustments can be morphological or chemical.

Degreasing of the surface is mandatory, because the cleanliness of the surface is directly related to the wettability, allowing for a better contact between the two materials. Degreasing of metals is generally performed using substances like isopropyl alcohol, acetone or methyl-ethene-kethone.[15] Degreasing of polymers can, besides the removal of a weak boundary layer, have the advantage to introduce functional groups that are often oxygen carrying. This is called the 'activation' of the surface. It increases the polarity and thus in this case the reactivity of the polymer. This can be obtained using flame treatment, corona discharge treatment or plasma treatment and can increase the initial adhesion by a tenfold.[16]

Mechanical treatments of the metal surface often result in a higher porosity and a rough surface on a macroscopic scale. These treatments are performed on the metal surface instead of the polymer surface because polymers are more prone to damage caused by these methods. Polymers are known to be able to penetrate these pores, as shown by Packham et al. for polyethylene on anodized aluminium, which can result in an increase of adhesion strength.[17] This increase in strength with an increase in pore size is, however, limited by an upper bound, as a too

large pore size will make the interface prone to corrosion and thus degradation.[18] As already mentioned, the degree to which mechanical interlocking and chemical bond formation contribute to an increased adhesion strength is still a matter of debate. Since recent literature proved the importance of chemical bond formation, it will be the main focus of this thesis.[9] Consequently to the increased possibility for chemical interaction, it was found that an increased roughness leads to an increased distribution of stresses, which allows for a possibility to take up an increased load. The mechanical roughening can be done using abrasive pads, grit-blasting or slurry-blasting always followed by degreasing.[19]

Chemical treatments are used for several reasons. It can be used to increase the surface free energy, increase the porosity by etching, introduce polymeric functionality, or provide a conversion layer that is stable, which can make sure that corrosion is inhibited throughout the lifetime of the material and optimized bonding conditions apply at the hybrid interface. Increasing the adhesion strength can also be obtained by varying the oxide or hydroxide fraction of the material. Wielant et al., for example, showed the strong correlation between the hydroxyl fraction on an iron oxide substrate and the number of adsorbed organic molecules. This allows for a certain degree of tunability, as an increased amount of alcohol groups was beneficial for the adsorption.[20] Similar results were obtained for aluminium oxide and zinc oxide substrates.[18,21,22] Copper could be hypothesized to behave similarly, but no so research is performed to this date. Copper oxide layers are spontaneously formed in our atmospheric conditions and the composition of this oxide layer can therefore be important for the application on the Pagoda.

3.2. Hybrid interactions on copper(oxides)

3.2.1. Theoretical background

Copper is a widely used material and has applications in the construction of buildings, technological applications, and transportation equipment. Copper can readily be used, since it forms a passivation layer in alkaline solutions that protects it from further corrosion, as can be seen in Figure 4.[23] This passivation layer can consist of different forms of copper oxide (CuO or Cu_2O) and can even be a patina, the passivation layer as obtained when the copper is exposed to ambient conditions, which can have phases such as cuprite, antlerite and brochantite.[24,25]

The surface state of metals is governed by both their inherent properties and the conditions they are in. Each metal has a corresponding Pourbaix diagram, which is a thermodynamic diagram that shows the possible phases a certain pH and polarization potential in an aqueous, electrochemical system. It allows to determine the stability of certain oxides at different potentials and pH. In Figure 4, the diagram of copper is shown. The oxidation of copper is possible at ever pH, starting from a potential of -0,6V. Copper oxides are stable in a wide pH range, and the type of oxide formed depends on both the potential and the pH.

Copper can thus be present in the form of metallic copper (Cu), cuprous oxide (Cu_2O), cupric oxide (CuO) and cupric hydroxide ($Cu(OH)_2$). The Cu_2O is said to originate from diffusion of Cu to the surface, where it interacts with the oxygen in the air. $Cu(OH)_2$ on the other hand is formed because of interactions of Cu with hydroxyl groups on the surface. Afterwards it is then transformed into the more stable CuO.[26] It is shown that this formation happens simultaneously and that the formation of the different layers is dependent on one another.[26]

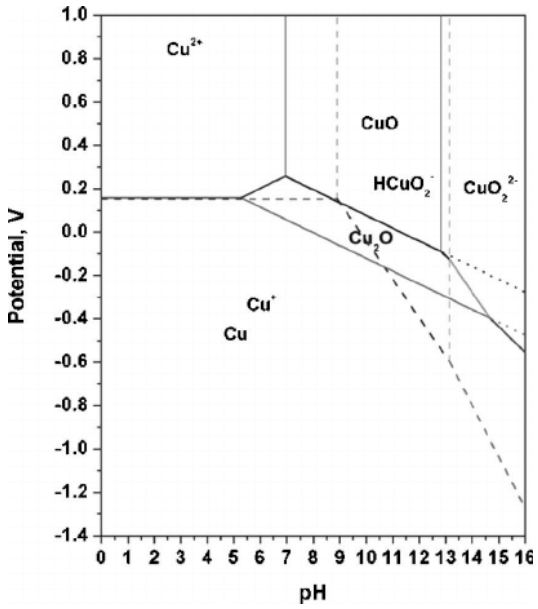

Figure 4 Pourbaix diagram of copper[23]

Copper oxides can be distinguished using X-ray photoelectron spectroscopy (XPS) measurements or Raman spectroscopy. A native oxide layer will give rise to several peaks, of which Cu2p and O1s are especially interesting for the characterization.[27] In order to distinguish $Cu^{(0)}$ and Cu_2O, the Cu_{LMM} peak should be analyzed as well.[28] The signature Cu2p, CuLMM and O1s peaks for copper and its oxides are shown in Table 2.[29]

Table 2: Position of signature peaks in X-ray photo-electron spectroscopy (XPS) spectra for the Cu2p, CuLMM and O1s peak

Cu2p	
Compound	Peak (eV)
$Cu^{(0)}$	932,6
Cu_2O	932,5
CuO	933,7
$Cu(OH)_2$ – as a shoulder	935,1
CuLMM	
Compound	Peak (eV)
$Cu^{(0)}$	568,0
Cu_2O	570,4
O1s	
Compound	Peak (eV)

Cu_2O	529,6
CuO	530,3
$Cu(OH)_2$	531,2

The Cu2p peak will thus allow to differentiate between $Cu^{(2+)}$ and $Cu^{(1+)}$, but not between $Cu^{(0)}$ and $Cu^{(1+)}$. To be able to distinguish those peaks, one must analyze the so-called Wagner plot, where the peak position of the Cu2p peak is plotted against the auger kinetic energy of the CuLMM peak, as shown in Figure 5.[30] The auger kinetic energy can be calculated from the binding energy of the CuLMM peak using Equation 1.

$$E_k L_3 M_{45} M_{45} = h.\nu - E_b - \varphi \quad (1)$$

$E_k L_3 M_{45} M_{45}$ is the auger kinetic energy

h is Planck's constant

ν is the frequency of the X-ray

E_b is the binding energy of the CuLMM peak

ϕ is the work function

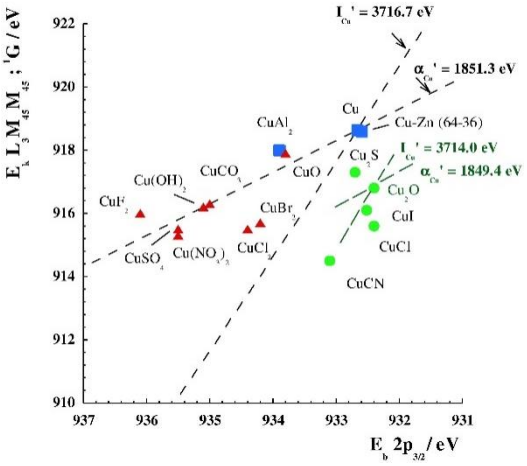

Figure 5: Wagner plot for copper [30]

Although copper is a very widely used material, insights on the interactions with organic materials are yet to be constructed. Most research papers aim at solving a specific problem, like the copper polymer hybrid interface in printed circuit boards (PCB's), but fail to elaborate on the mechanism that is at play.[31] Other applications of interactions of copper with organic materials are conductive coatings and microelectronic packaging.[32–34]

3.2.2. Production of copper oxides

To be able to study the effect of different oxides on the adhesion behavior, stable oxides must be produced. From the Pourbaix diagram, it is already known that $Cu(OH)_2$ is a metastable phase and will therefore be difficult to isolate. Alkaline solutions, such as NaOH can allow for the production of either cuprous or cupric oxides, depending on the duration of submersion and induced current.[35,36] The oxides can also be obtained by heating the sample. Since cuprous oxide is more stable, it will be produced at lower temperatures (3h at 300°C) than cupric oxide (3h at 350°C). These results can be verified using X-ray diffraction (XRD) spectra.[37] $Cu(OH)_2$ is often produced as a powder, but recent literature suggests a method based on $CuSO_4$ and NH_3 to chemically deposit a thin layer of $Cu(OH)_2$. The mechanism is shown in Equations (2) to (4). The resulting layer is amorphous.[38]

$$Cu^{2+} + OH^- \rightarrow Cu(OH)_2 \quad 2$$

$$Cu(OH)_2 + 4NH_3 \rightarrow Cu(NH_3)_4^{2+} + 2OH^- \quad 3$$

$$Cu(NH_3)_4^{2+} + 2OH^- \rightarrow Cu(OH)_2 + 4NH_3 \quad 4$$

3.2.3. Interaction with copper oxides

The most well-known pretreatment for adhesion of organic material on copper substrates is the formation of black oxides, which is a type of conversion coating where the copper substrate is converted to cupric oxide (CuO).[31,33,39] Dynamic secondary ion-mass spectrometry analysis showed that, after heat treatment and production of the black oxide, the oxide layer actually consisted of two types of oxides: a cupric oxide that was about twice as thick as the underlying cuprous oxide (Cu_2O) layer. The oxide layer is not discontinuous, as the outside layer consists of a layer made of mainly cupric oxides, while the amount of cuprous oxide will increase gradually when going deeper into the oxide layer. Adhesion failure seemed to occur due to a failure in inside the oxide itself, unless the oxide was sandblasted. [40]

Another example of an organic material the is known to interact with a cupric oxide surface is polyethylene. Research showed that CuO is more prone to react with polyethylene than Cu_2O, because of its ability to oxidize this polyethylene. The importance of the substrate topology was shown, by reducing it in an electrolytic process, as the adhesion strength remained high.[41] In earlier days, the adhesion of polyethylene on copper oxides was a well-researched topic, but no recent papers discuss this phenomenon.[42,43]

Silane groups were shown to interact with copper hydroxides, through a condensation reaction between (-Si-OH) and (-CuOH).[44] These silanes can act as SAM's or as a conversion layer for further adhesion of organic coatings.[45–47] The effect of the hydroxyl fraction on the adhesion strength was not reported.

3.2.4. Interaction with metallic copper

Benzotriazole, which is interesting as a conducting coating, is known to self-assemble on copper (the mechanism is shown in Figure 6). A connection can be formed with epoxy-functionalized polymers to form a thicker coating.[48–50] A complete review of different types of azoles, their corrosion inhibitor properties and the preferred conditions was performed in literature, reporting the corrosion efficiency by characterization using the storage modulus and UV spectroscopy.[50,51] The review, however, lacks information on the mechanism behind this reaction.

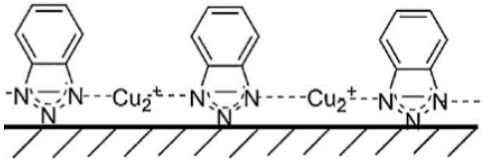

Figure 6: Self-assembly of benzotriazole on copper metal [50]

Benzotriazole is, however, toxic and cannot resist to high temperatures and potentials, which is why poly(o-anisidine) was successfully used to create self-assembling layers on pure copper that showed corrosion protection properties. The results were verified using a combination of Fourier-transform infrared spectroscopy (FTIR), Electrochemical Impedance Spectroscopy (EIS) and Cyclic Voltammetry (CV).[52] Similar results were obtained for polyaniline.[53]

Marcus et al. performed extensive theoretical and experimental studies to better define the interaction mechanism between copper and azoles, combining DFT calculations, Auger electron spectroscopy (AES), scanning tunneling microscopy (STM) and XPS measurements.[54–57] The analyzed surface was a Cu(111) surface with an ultrathin Cu_2O(111) film and the adsorbed molecule was 2-mercaptobenzothiazole (MBT). The copper surface was modelled as shown in Figure 7, where Cu_{csa} and Cu_{cus} correspond to respectively the saturated and unsaturated copper and O_{up} and O_{dw} correspond respectively to the unsaturated and saturated oxygen compounds. Some important hypothesis were made using DFT calculations: (i) for small concentrations, the MBT molecule orients horizontally to the surface and is chemically bound to the substrate by an interaction between sulfur and the Cu_{cus}, while the nitrogen interacts with the Cu_{csa}, (ii) for higher concentrations, the azoles formed a densely ordered monolayer perpendicular to the surface and (iii) the same mechanisms were found for anhydrous, hydrated and hydroxylated surfaces. Contradictory to the findings on aluminium, the substitution of hydroxyl compound is even unfavored.

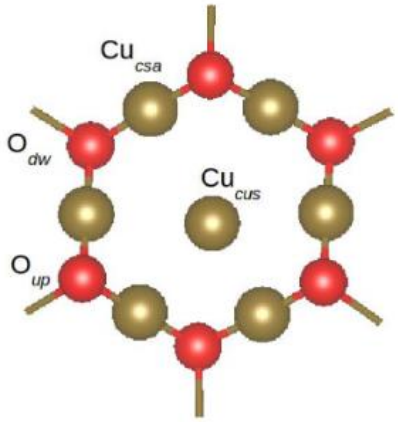

Figure 7: Schematic representation of the Cu_2O surface, where O_{up} and O_{db} correspond to the unsaturated and saturated oxygen respectively and the Cu_{cus} and Cu_{csa} correspond to the unsaturated and saturated copper sites respectively.[57]

These results were verified by XPS measurements, as the S1 and S2 components (corresponding to the bound and unbound thiols at 162 eV and 163 eV respectively) of the S2p peak and the N1 and N2 components (corresponding to the unbound nitrogen and the nitrogen that is part of a Lewis-type interaction respectively) of the N1s peak changed for different degrees of exposure. By comparing their relative contributions to the stoichiometric ratio in the MBT molecule, the findings from the DFT calculations were confirmed.[54] This is an interesting method for analyzing and characterizing reaction mechanisms using XPS.

The thickness of the adherend MBT film depends on the pH. Only at a pH below 3, when the Cu_2O layer is instable, can the organic film be thicker than a monolayer without the dissolution of copper ions. The Cu_2O layer thus passivates the surface from further interaction.[58]

Another important interaction is the one between metallic copper and thiols. Thiols are used to improve the adhesion between copper and epoxy.[59,60] As already mentioned, the pure copper is preferred due to its electron density, which was illustrated by the lack of encapsulating layer at room temperature and a presence at 75°C, when CuO is partially dissolved.[12,61]

A final example of an organic species interacting with metallic copper is polyacrylonitrile. It was shown, using a combination of DFT calculations and XPS-measurements that there is a chemical interaction between the copper and the nitrogen and carbon atoms. The interaction was said to be a di-σ adsorption of the terminal C and N atoms of the polyacrylonitrile.[62]

3.3. Gold

3.3.1. Use of glued gold in art and cultural heritage

Gold has been used as a decorative element throughout history to cover a wide variety of artefacts made of stone, metal and glass. The use dates to the gilding of the sarcophagus of the ancient Egyptian pharaohs and the temples of former Chinese civilizations. Today, it is still used in cultural heritage that mark our society, such as the golden gates of Versailles and many other statues spread throughout Europe. Historically, however, the thickness of the gold was kept as thin as possible, as it seemed to improve the durability of the layer and the efficiency of the use of the material. The art of thinning the material has been as much a challenge throughout the history as the gilding itself.[63] This is in contrast with the gold on the Pagoda, which is not only one of the largest gilded monuments in history, but also contains much thicker golden sheets. The gold is an illustration of the abundance of the noble metal, as well as the devotion of the Buddhists to their way of life.

Because of the importance of the evenness of the substrate, the gold was often applied on a primer called a 'Gesso'. Gilding would historically be performed with three different types of adhesives, (i) natural oils such as linseed oil, (ii) glucid adhesives such as honey or (iii) protein based adhesives like animal glues.[63,64]

Diffusion bonding, on the other hand, can also be used to gild materials. In diffusion bonding, the gold is thought to adhere due to an interdiffusion process. This can be performed using thermal processing, hammering of the gold or fire gilding. In fire gilding, the gold is mixed into a so-called amalgam with mercury and applied to an etched surface after which the mercury will be evaporated.[64] This fire gilding is also used on the pagoda, but remains a less interesting solution due to the high toxicity of the mercury. There is a lot more information to be found, for which the reader is referred to other extensive review papers (such as those by Oddy et al.[64]). However, it is

interesting to note that research regarding the chemical interaction between gold leaf and adhesives for its use in cultural heritage has yet to be performed.

Natural oils mainly consist of alkanes that are functionalized with carboxylic acids, as shown in Figure 8.

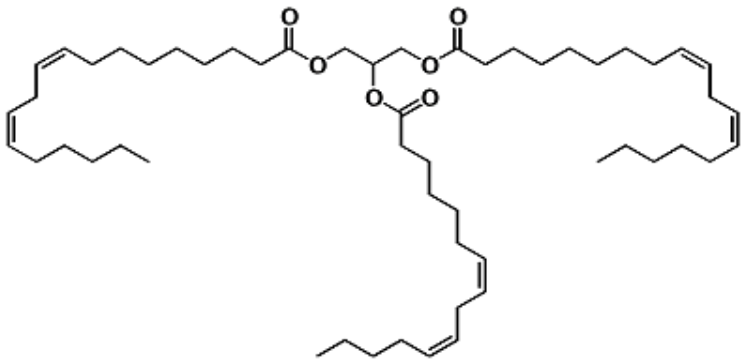

Figure 8: Chemical composition of linseed oil [63]

3.3.2. Theoretical background

Gold is known as a noble metal since it doesn't react with other elements under ambient conditions. It is often used for technological applications because of its outstanding electronical and thermal conductivity. To be able to grasp the reactivity of gold, one can examine the Pourbaix diagram as shown below in Figure 9. Gold can only be oxidized above the potential defined by the oxidation of water to oxygen. Because of this, gold cannot be oxidized when brought into contact with dissolved oxygen and in extremely basic or acid conditions, since the oxygen would be transformed into water. Gold acquired the title of most noble of all metals, because it is the only metal that has this specific characteristic. [65]

Research shows that these properties change in the nanoscale range and that gold will become much more active. This is confirmed by the fact that the melting point of gold decreases when the particles are smaller than 3 to 4 nm. It is because of this that gold is so interesting for catalytic applications.[65]

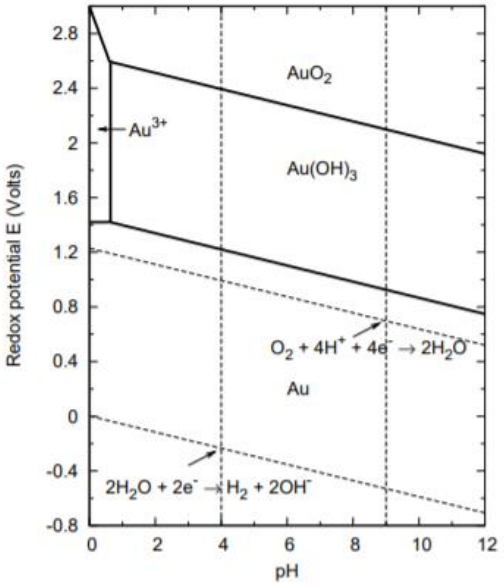

Figure 9: Pourbaix diagram of gold [65]

Gold can be oxidized when brought into contact with both specific ligands and an oxidizing agent. The oxidation of gold can happen through two different reactions $Au \rightarrow Au^{+}(aq) + e^{-}$ or $Au \rightarrow Au^{3+}(aq) + 3e^{-}$. The fact that this reaction only happens in the presence of both a ligand and an oxidizing agent, can be seen in the absence of reaction of gold and oxides and the presence of reaction of gold and aqua regia. Hydrochloric acid will act as an oxidizing agent and nitric acid as a ligand.[66]

$$Au\ (s) + 3\ NO_3^-(aq) + 6\ H^+(aq) \rightarrow Au^{3+}(aq) + 3\ NO_2(g) + 3\ H_2O(l) \qquad 5$$

In general; [67]

$$Au\ +\ 2X^- \rightarrow\ [AuX2] +\ + e^- \qquad 6$$

$$Au\ +\ 4X^- \rightarrow\ [AuX4]^{3-} +\ + 3e^- \qquad 7$$

It is this ability to form complexes with Au(I) and Au(III) that determines the properties of a bond formation. In the presence of a stronger ligand, such as chlorides, can increase the stability domain of oxidized species.[65]

3.3.3. Interactions with gold

An important next step is to connect this theoretical information to experimental work. Over the last twenty years, reviews showed that gold offered much more possibilities than first assumed given its noble character.[68,69] Due to a variety possible of covalent interactions, gold is widely researched as a catalyst for organic material.[70,71]

A well-studied example is the self-assembly of thiols on gold surfaces.[72–75] Depending on the side chain of the sulfur-group, different degrees of reactivity were obtained regarding the interaction with copper complexes.[72] The suggested mechanism is the following;

$$R - SH + Au_n^0 \rightarrow RS^- - Au^+ + \frac{1}{2}H_2 + Au_{n-1}^0$$

The suggested mechanism consists of a chemical bonding after diffusion and subsequent self-assembly under the influence of Van Der Waals forces; the S-H bond is oxidized and will bind to the gold, after which hydrogen is reduced. The strength of the originated bond was measured to be 48 kcal/mol.[76] Later research suggested that this mechanism was a simplification, as the electron transport will also depend on the grain orientation of the gold and the length of the thiol chains. .[77,78] If the thiol molecule is functionalized with, for example, carboxylic acid, this can allow the formation of subsequent strong interactions with polymers.[79] The covalent interaction was characterized using XPS for different chain constitutions and the Au/S ratio was used to define the coverage of the sample.[80,81] The C/S ratio was used to evaluate the presence of thiolic compound by comparing it to the stoichiometric of the used thiol.[80]

Although thiols are a first resort when it comes to forming covalent bonds with gold, the theory suggests other possible interactions if a ligand and an oxidizing agent are present.[69,71] The research regarding the interaction with other elements is, however, rather preliminary and limited to nanostructures. It is important to consider that a pure gold surface might not interact the same way as gold nanoparticles.

The Au-C bond is one of these alternatives and showed an adhesion strength up to 255 kJ/mol.[82,83] The mechanism, however, is not yet fully understood.[70] This again shows the gap in knowledge between the purely theoretical and applied research. The possible formation of these bonds has led to a whole new range of research, where gold can be embedded into polymer chains, like polyethylene.[84] The alkane chains were even shown to self-assemble on the gold surface. If these chains are terminated with functional groups, such as carboxylic acids, they can be used as a basis for further adhesion with other monomers and polymers.[85] Interaction with carboxylic acid groups can also occur and gold can therefore be used to adhere carboxylic acids to alkynes.[86] The adsorption of carboxylic acids on gold, however, requires an anodic current.[74]

An Au-O bond can be formed if atomic oxygen is in a trifold state. This atomic oxygen can be created by the dissociation of O_2 due to the rough substrate. This adhered oxygen can be interesting for use as a catalyst, as It might oxidize CO, olefins and might induce oxidative transformations.[87] This can in turn be interesting for chemical bond formation with other monomers or polymers.

3.4. Possible causes of delamination

Once a good adhesion is obtained, the formed connection must be durable. There are many possible causes for delamination, and they must all be mitigated to increase the lifetime of the joint as much as possible.

One of the possible causes is electron transport away from the copper metal, when the metal is oxidized. This can be caused by a galvanic contact, but also due to electron transport to the more noble gold substrate when evaluating the gluing of gold onto copper. Water intrusion can also cause corrosion issues.[88] Another important factor is the chemical structure of the oxide layer. Adhesion failure can occur in the oxide layer if there is a mismatch in the $Cu/Cu_2O/CuO$ interface.[89] On top of this, the internal microstructure is known to change over time and in the presence of heat.[90] This is, however, outside of the scope of this thesis.

The delamination of gold cannot be caused by oxidation, as the conditions for the oxidation of gold are much more extreme than those encountered on the pagoda.[91] The gold could, however, delaminate due to stresses caused by thermal expansion which are larger than the strength of the chemical bond formed between gold and the adhesive.

4. Methodology

Current research is clearly unable to provide solutions for the delamination issue on the Pagoda. Although there are many suitable organic molecules for bond formation with copper surfaces, it is unknown to what extend the type of copper oxide can influence the adhesion strength and thus how corrosion can induce delamination. On top of this, research regarding chemical bond formation with gold is mainly limited to theoretical descriptions. This research aims to better understand the difference adhesion strength of a metal-organic interface for metals with unassociated properties.

4.1. Materials

Gold from Myanmar was provided as a pure sample (rolled in the factory), glued onto copper before it was mounted on the temple (Figure 10, b) and as a part of a sample that spent five years on the temple (fire gilded, not glued - Figure 10, c). The samples were used as received. As a model gold substrate, an electrode was used (Figure 10, a), which was polished in between submersion tests. To remove impurities from the substrate, the gold was cleaned with ethanol.

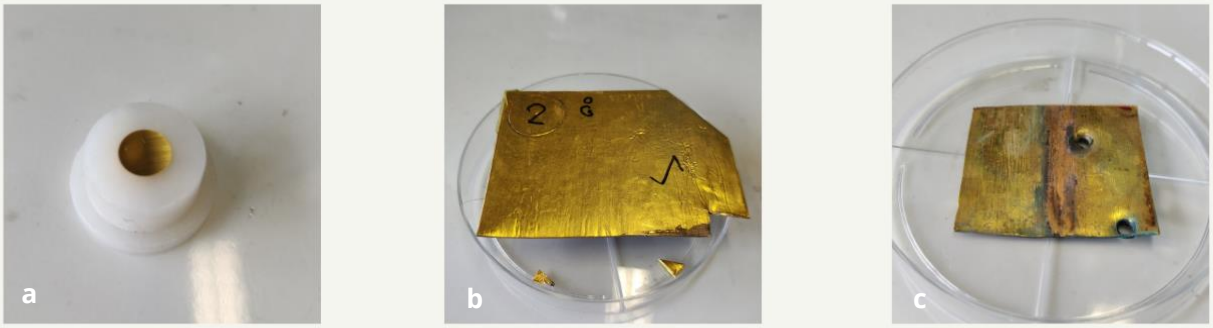

Figure 10: (a) Gold electrode used as bare gold substrate for testing, (b) unused glued gold on copper from Myanmar and (c) used fire gilded gold plate.

Copper from Myanmar, was provided as a sample (Figure 11,b), glued onto gold before it was mounted (Figure 11,c) and as a part of a sample that spent five years on the temple (fire gilded, not glued). These samples were used as received. Model copper (Figure 11, a) samples were provided by Goodfellow. To remove impurities, the samples were cleaned with acetone and afterwards subsequently submerged in acetone and ethanol (both 99% purity) in an ultrasonic bath filled with milliQ water for 10 minutes.

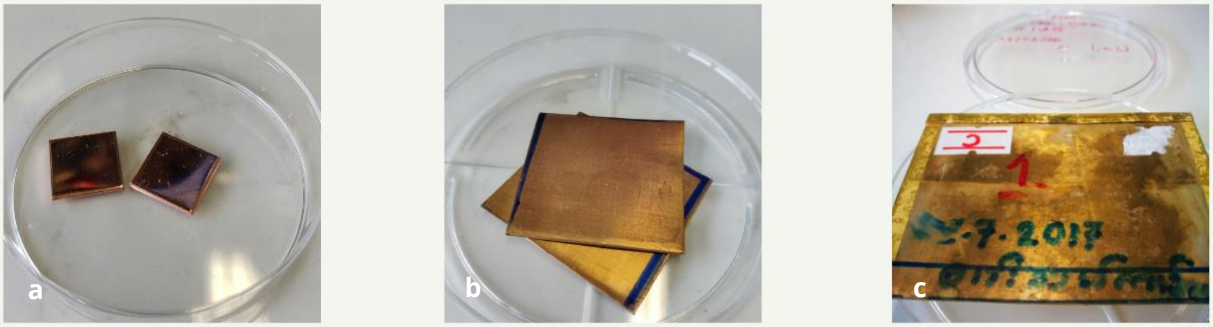

Figure 11: (a) Bare copper substrate used in the lab, (b) bare copper substrate from Myanmar and (c) unused gold glued on copper.

Model molecules and glues, namely diethylenetriamine (99% purity), succinic acid (>99,5% purity) and 1-octanethiol were provided by Sigma Aldrich and are shown in Table 3. The glue used for the temple in Myanmar was provided by Huntsman.

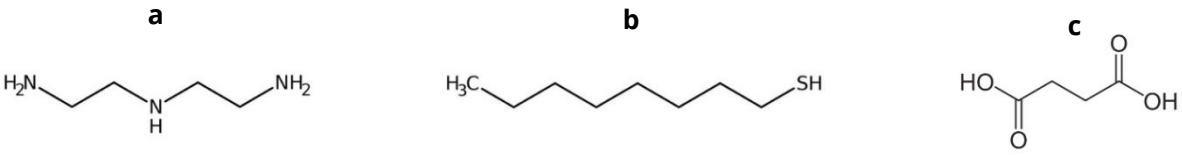

Figure 12: Chemical structure of (a) DETA, (b) 1-octanethiol and (c) succinic acid

Solvents, namely tetrahydrofuran (THF), ethanol (99% purity) and milliQ water were provided by Millipore Corporation and Sigma Aldrich respectively. All used materials were summarized in table 3.

Table 3: Used materials throughout tests and characterizations

Type	Origin
Gold 1 cm x 1 cm	Goodfellow
Damaged gold and copper plate	Myanmar
Gold 1 cm x 1 cm	Myanmar
Fire gilded gold on copper	Myanmar
Gold glued to copper	Myanmar
Copper 1 cm x 1 cm	Goodfellow
Copper 4 cm x 3 cm	Myanmar
Huntsman glue	Huntsman (by Myanmar)
DETA	Sigma-Aldrich
Succinic acid	Sigma-Aldrich
1-octanethiol	Sigma-Aldrich

4.2. Research questions and methodology

The main research question is the following:

How can we provide a high adhesion strength in a system that contains metals with unassociated properties?

This question can be subdivided into three subsections.

1 What are the surface characteristics of copper and gold in ambient conditions?

To understand the specific adhesion issues, the surface of both metals must first be characterized. For gold and copper, it is important to know the degree of purity. For copper the type of oxides and their respective ratio are crucial to understand the mechanism behind bond formation. Both these factors can influence the bond formation and durability.

The Burmese Minister of Culture provided samples from the pagoda, used and unused, as well as a sample of the Huntsman glue. First, the received materials will be analyzed using optical microscopy to learn more about the application of the glue. Since covalent bond formation is very surface sensitive, the main interest will be the top layer of the received metals, which will be analyzed using XPS measurements. The copper and gold from our laboratory will also be analyzed using XPS and possible differences will be documented. Further tests will be performed on the material from the laboratory, since the received samples from Myanmar are limited.

2 What model molecules interact with both the copper oxide system and the pure gold?

Model molecules will be used to mimic adhesives, as the interfacial interaction can only be characterized using XPS if the organic layer on the substrate is very thin, due to its small depth resolution (about 7 nm). As an introduction to this section, model molecules based on the Huntsman glue will be used. A DETA solution of 0,1 wt.% in tetrahydrofuran (THF) will be prepared and the samples will be characterized using high resolution XPS spectra. Both copper and gold will be submerged for 30 minutes. Each iteration, two samples are prepared, where one is rinsed, and one is not. The samples were dried using nitrogen gas. ToF-SIMS will be performed to better understand the forming of complexes between copper and DETA. To learn more about the mechanism behind bond formation on copper, a higher concentration of DETA will be used to submerge samples (0,3 wt.%, 0,4 wt.% and 1 wt.%). The samples will be characterized using IR-spectroscopy to see the difference between chemically and physically adhered species. The lowest

concentration for which physically adhered species are present, will be characterized using XPS. This methodology is used, as the XPS requires a low number of non-adherend species to not contaminate the vacuum chamber, but the peak decomposition of the N1s peak requires both chemically and physically adhered species, in order to perform a relative peak fitting.

1. **What can we learn from glues used in cultural heritage?**

The functional group of natural oils is carboxylic acid and that is why succinic acid (0,1 wt.% aqueous solution) will be used as a model molecule to mimic the behavior of the natural oils. Gold and copper will be submerged for 30 minutes. The surface will be characterized using high resolution XPS spectra.

2. **What can we learn from glues used in industrial settings?**

Other atoms and molecules were shown to interact with both gold and copper. Literature showed that thiol-based compounds can be a suitable candidate for both copper and gold. Both metals will be submerged in a thiolic solution following a procedure was based on that of Urcuyo et al.[72], which analyzed the alkanethiol bond formation using XPS. A 1 mM ethanolic solution of 1-octanethiol was prepared and both samples were submerged for 1h and 24h respectively. The samples will be characterized and compared using high resolution XPS spectra.

3 How can this interaction be improved by changing the surface state of copper?

Literature also stated the importance of the presence of a copper oxide layer, as it might improve or reduce the adhesion properties. A cuprous and cupric oxide layer will be prepared using a controlled oven (Mettler Toledo) by heating for 3h at 300°C and 350°C respectively. First, heating is performed in an uncontrolled oven and afterwards the samples are heated un the controlled over, where both heating and cooling are performed at a rate of 10°C/min.

The different produced copper oxide layers will be submerged in the 1 mM ethanolic 1-octanethiol solution for 1h and characterized using high resolution XPS spectra.

4.3. Application procedure of different surface analytical methods

4.3.1. X-ray Photo-electron Spectroscopy

X-ray Photo-electron Spectroscopy (XPS) measurements were acquired using a PHI-Versaprobe II spectrometer with an Al Kα monochromatic X-ray source (1486.71 eV at 24,9 W) under a vacuum of approximately 5.10^{-9} Torr. Both surveys (in high sensitivity) and multiplex (in high-resolution) spectra were acquired for all encountered atoms (Cu, Au, C, O, N, S). The surveys were performed using a 280 eV pass energy, 1 eV step size and a scan window ranging from 0 eV to 1400 eV. The high-resolution spectra were performed using 26 eV pass energy, 0,05 eV step size and an adjusted scan window. The acquisition time was 15 min. per sample, leading to an average measurement time of one hour per sample holder. A neutraliser was used, and the measured area was 100 µm in diameter. Sputter profiles were acquired using a monoatomic Ar source (1kV or 3kV) for a sputter area of 3x3mm The XPS data was processed using CasaXPS (v.2.3.23). The calculated atomic concentrations are based on the experimental sensitivity factors and the transmission factors provided by the manufacturer. For each sample, two to three measurement points were acquired.

4.3.1.1. Peak decomposition procedure in CasaXPS

The energy scale was calibrated relative to the C-C, C-H binding energy of the C1s peak at 284,4 eV and a Shirley type background subtraction was used. The used line shape is Gaussian-Lorentzian 30 (GL(30)). The organic contamination was fitted using the C1S peak, according to the procedure suggested by Taheri et al.[92], meaning that the C-C, C-H peak was left free to fit, the C-COOH peak was fitted at 0,5 eV above the first peak, the C-O peak was fitted at 1,5 eV above the first peak, the C=O was fitted at 2,9 eV above the first peak and the O-C=O peak was again left free to fit. All peaks were supposed to have the same full width at half maximum (FWHM), as can be seen in Figure 13. The sole contribution of contamination can only be fitted for the bare substrate, as interactions will influence the C1s peak.

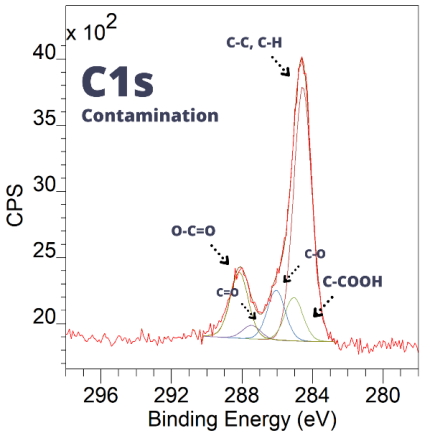

Figure 13: Peak fitting procedure for carbon contamination using the C1s peak.

The O1s peak was decomposed into an O_2^- contribution, OH^- contribution and a contribution made by CO_2 and H_2O, as suggested by Abrahami et al, as shown in Figure 14.[93] The OH^- and CO_2 peaks are separated at respectively 1,1 eV and 2,4 eV from the O_2^- peak. The FWHM is fitted to 1,8 (O^{2-}), 1,7 (OH^-) and 2,0 (CO_2) analogue to Abrahami et al. [93]

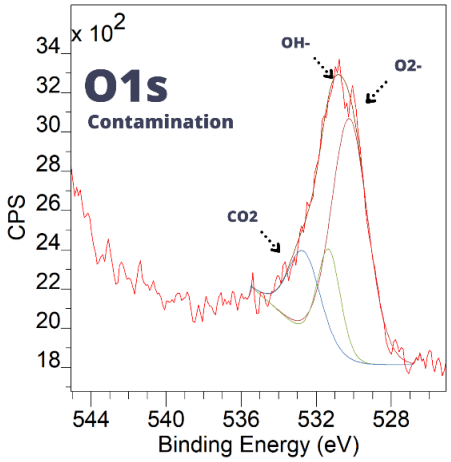

Figure 14: Peak fitting procedure of the O1s peak

The interaction with DETA was analyzed using the N1s peak, dividing the different types of contribution into N1 (physically adsorbed species or weak Lewis-type acid-base interactions), N2 (Lewis-type acid-base interactions) and N3 (Bronsted-type acid-base interactions) as suggested by Abrami et al.[93] The N1 peak was left free to fit, while the N2 peak was fitted at 1,5 eV above the first peak and the N3 peak was fitted at 3,8 eV above the first peak. All peaks were supposed to have the same full width at half maximum (FWHM), as can be seen in Figure 15.

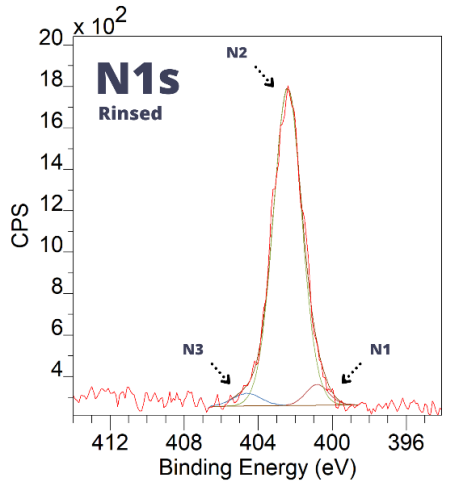

Figure 15: Peak fitting procedure for the interaction amines using the N1s peak.

The interaction with carboxylic acid was also fitted using the C1s peak using the procedure suggested by Pletincx et al.[94], meaning that the C-C, C-H peak was left free to fit, the C-COOX peak was fitted at 0,4 eV above the first peak, the C-OH peak was fitted at 1,7 eV above the first peak, the COO^- was fitted at 3,4 eV above the first peak and the C-COOX was fitted at 4,2 eV above the first peak. All peaks were supposed to have the same full width at half maximum (FWHM), as can be seen in Figure 16. The COO^-/C-COOX ratio is used as a measure for the relative amount of interacting carbonate species.

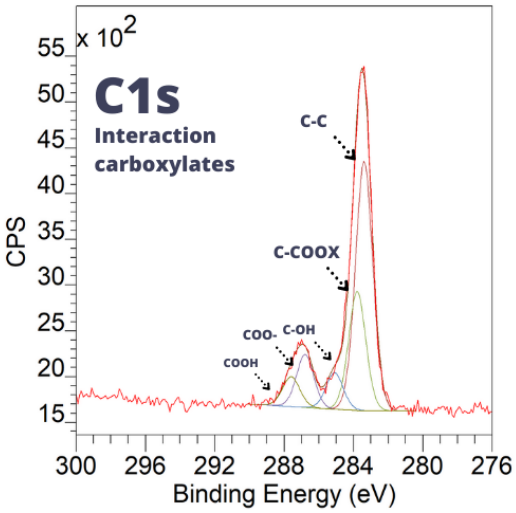

Figure 16: Peak fitting procedure for the interaction with carbonate species using the C1s peak.

The interaction with thiols will be fitted using the procedure as suggested by Urcuyo et al, as illustrated Figure 17.[72] Thiolates give rise to a peak at lower binding energies (162 eV), while unbound thiols give rise to a peak at higher binding energies (163 eV). The peaks were constrained to 0,2 eV compared to their original position and have the same FWHM.

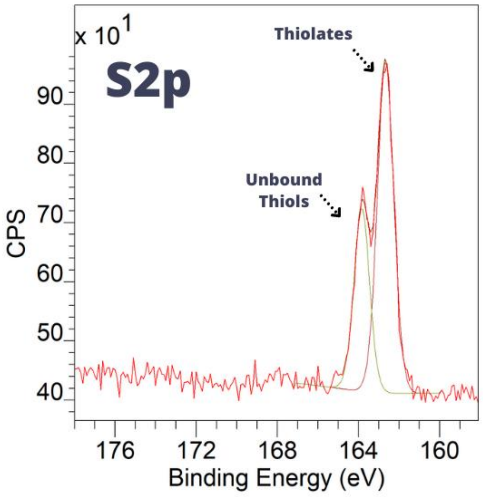

Figure 17: Peak fitting procedure for the interaction with thiolic compounds using the S2p peak

4.3.1.2. Calculation of the hydroxyl fraction in MATLAB®

The hydroxyl fraction was calculated as suggested by Hauffman et al.[95], using the relative contributions of the O-C=O and C-O areas of the C1s peak and the OH^- and O_2^- areas of the O1s peak. The hydroxyl fraction was calculated as follows

$$hydroxyl\ fraction = \frac{1}{1 + \frac{C_{O^{2-}}}{C_{OH^-}}}$$

The concentrations can be calculated from the peak intensities using

$$I = F\sigma \int c(x) \exp\left(-\frac{x}{\lambda sin\theta}\right) dx$$

where F is a factor that contains all instrumental factors, σ is the photo-ionization cross-section, λ is the inelastic mean free path (IMFP) and θ is the measured angle. The used values and their origins are reported in Table 4. The IMFP was determined for a kinetic energy of 918 eV.

Table 4: Factors used for the estimation of the hydroxyl fraction in copper oxide surfaces.

Factor	Value	Source
Photo-ionization cross-section σ_C	0,157	Yeh et al.[96]
Photo-ionization cross-section σ_O	0,04	Yeh et al.[96]
Inelastic mean free path λ_C	23	NIST database, TPP method[97]
Inelastic mean free path $\lambda_{O,organix}$	23,62	NIST database, TPP method[97]
Inelastic mean free path $\lambda_{O,oxide}$	17,28	NIST database, TPP method[97]

The intensities are both related to the thickness of the contamination layer, which allowed to use an algorithm build in MATLAB® to minimize the error between the calculated intensity ratio and the experimental data.

4.3.2. TOF-SIMS

Secondary ion mass spectrometry (SIMS) analysis of the samples surface was performed using an ION-TOF TOF.SIMS 5 instrument equipped with both Bi-Mn Nanoprobe-LMIG (liquid metal ion gun) and Cs/O2-DSC (dual source column) primary ion sources mounted at 45° to the surface normal. The secondary ions were collected by a reflection-type time-of-flight (ToF) mass analyzer perpendicular to the sample surface. Mass spectra were obtained by scanning a pulsed 30-keV Bi3+ beam (current: 0.35 pA), operated in high current bunched mode for high mass resolving power on 200 × 200 µm2 sample areas, at 128 × 128 pixels. The analysis time was 60 s, keeping the total ion dose below the static limit of 1 × 1013 ion·cm-2. ToF-SIMS spectra were acquired in both ion polarities. Three to five measurements per polarity were carried out for each sample. All

data processing was carried out using the software supplied by the instrument manufacturer, SurfaceLab (version 7.1).

4.3.3. Raman Spectroscopy

The Raman spectroscopy apparatus is a Labran HR evolution (Horiba). A green laser (532 nm) was used at 10 % (~1mW) and the objective was adjusted to obtain the best resolution. The image was enlarged 100 times and a confocal lens was used. The apparatus has a micron-size lateral and depth resolution.

4.3.4. IR Spectroscopy

The FTIR apparatus is a Thermo-Nicolet Nexus equipped with a liquid-nitrogen cooled mercury-cadmium-telluride (MCT) detector and a nitrogen-purged measurement chamber with a Veemax III single reflection ATR accessory. In order to study the physisorption of the DETA molecule on the copper surface at different concentrations, grazing incidence reflection adsorption (RA) spectra were recorded. To this purpose, IR-light was configured with an incident set angle of 80 degrees (angle from the plane normal). Infrared backgrounds were obtained from the copper substrate cleaned with acetone and ethanol. Infrared spectra were collected from 128 cycles with a resolution of 4 cm-1. The control of the spectra acquisition and incident angles was managed by the OMNIC 9.9.473 software package (ThermoElectron Corporation, Madison, WI). Finally, atmospheric suppression as well as a manual baseline correction based one the wavenumbers 4000 cm^{-1}, 3600 cm^{-1} , 2800 cm^{-1} , 2500 cm^{-1} , 1000 cm^{-1} and 800 cm^{-1} were performed.

5. Results

5.1. Study of the surface of used metals

The surfaces of both copper and gold will be examined to better understand their chemical composition. The model samples will be compared to those received from Myanmar, to verify the validity of their use.

5.1.1. Study of the oxide layer of different copper surfaces

The surface of the copper substrate (model system) provided by Goodfellow Inc. will be compared to that of the copper received from Myanmar. The composition of the oxide layer is very important for the possible chemical interactions and must therefore be evaluated.

5.1.1.1. Examination of the oxide layer of the model copper from Goodfellow

The copper received from Goodfellow Inc. will be used as model system for all further adhesion testing. The oxide layer will therefore be evaluated. For this, high-resolution XPS spectra of the individual elements that are found in this oxide layer (O1s, C1s, Cu2p and CuLMM peaks) will be measured. To understand the difference between oxides on the surface and the oxides deeper in the structure, the material was sputtered using a monoatomic argon source. The sample was sputtered for one minute. The sputter rate is assumed to be similar to that of SiO_2 (3,5 nm/min), meaning that the depth of the measurement after sputtering for one minute is equal to 3,5 nm.[98]

To be able to describe the copper surface entirely, the O1s peak must be examined first. The different contributions to this peak will allow us to identify the presence of copper oxides (around 530 eV), hydroxides (+1-1.5 eV) and carbonates and/or adsorbed water (+3 eV). However, oxygen coming from the organic contamination inevitably present at the surface also contributes to this peak. Therefore the true hydroxyl fraction must be calculated from the -OH subpeak at around 531 eV after substraction of the organic oxygen contribution assuggested by Hauffman et al.[95], and indicated in the experimental section. The contamination contribution can be evaluated after decomposition of the C1s peak (i.e. from the C-O_x components). The Cu2p peak can be used to differentiate between $Cu^{(2+)}$ and $Cu^{(1+)}$ (or $Cu^{(0)}$), as $Cu^{(2+)}$ will cause a sattelite peak around 942 eV (for both CuO and $Cu(OH)_2$). Finally, a Wagner plot based on peak position of the CuLMM peak allows us to distinguish between $Cu^{(0)}$ and $Cu^{(2+)}$.

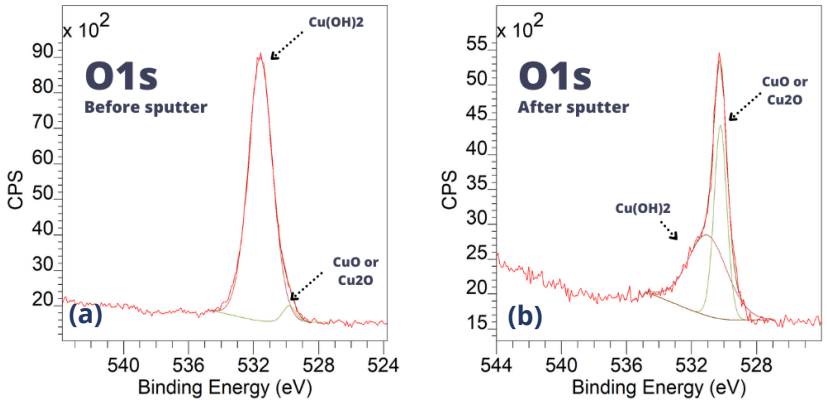

Figure 18: High-resolution XPS spectra of the O1s peak measured on model copper (a) before sputtering and (b) after one minute of sputtering. The different contributions are illustrated by the decomposition of the peak in a contribution at 532 eV $(CuOH)_2$ and 530 eV (CuO or Cu_2O).

Figure 18, the O1s peaks measured on the unsputtered surface (a) and the sputtered surface after 1 min 1-keV Ar^+ etching (b) are compared. The O_{1s} peak has two contributions for both samples, one around 532 eV which is typically identified as a $Cu(OH)_2$ contribution and one at 531 eV, which indicates the presence of either CuO or Cu_2O (it is not possible to distinguish these two oxides here). The unsputtered surface (a) clearly shows a larger hydroxide contribution. The OH-fraction was calculated using the atomic percentages of O-C=O, C-C-O, OH and O^{2-} by performing a peak decomposition on the O1s and C1s peak as described in section 4.3.1.2. These peak decompositions are shown in Annex 9.1. The OH-fraction is equal to 21% for the bare sample and 0% for the sputtered sample, meaning that the topmost hydroxide layer has been completely removed by 1-keV Ar^+ etching.

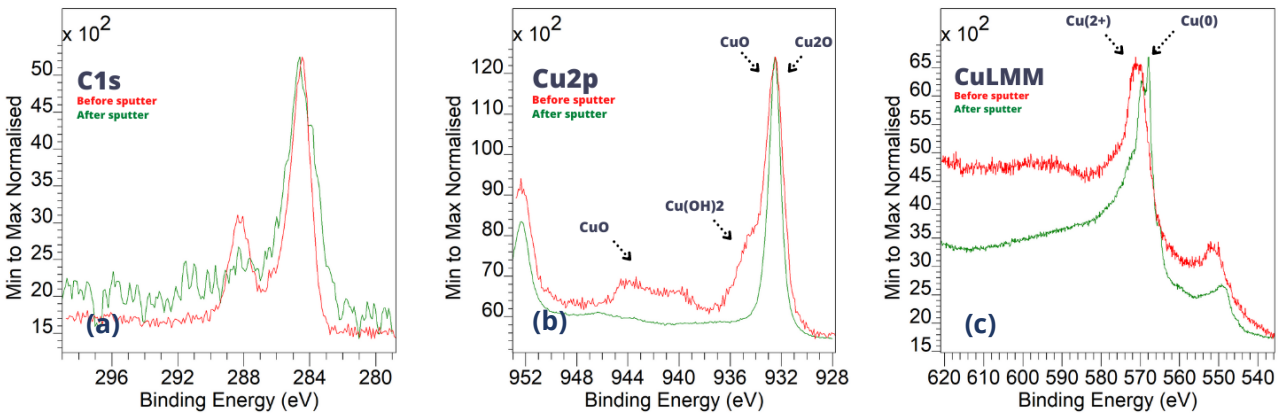

Figure 19: High-resolution XPS spectra of model copper sample: the (a) C1s peak, (b) Cu2p peak and (c) CuLMM peak. The sample was sputtered for one minute. The red spectra refer to the sample before sputtering and the green spectra to the sample after sputtering.

Figure 19 shows the high-resolution measurements of the C1s (a), Cu2p (b) and CuLMM peak (c) for the model copper sample before sputtering (red) and after sputtering (green). The C1s peak is min to max normalized. The C1s peak of the sputtered sample (a, green) is noisier, illustrating that there is relatively less carbon present deeper in the oxide layer, as the original (i.e. before normalization) peak is much lower. The Cu2p peak (b) shows a single peak at 932 eV for the sputtered surface (green), while the spectrum of the top surface (red) clearly shows a shoulder at 935 eV and a sattelite peak at 942 eV. The peak at 932 eV signifies the presence of Cu_2O (or Cu(0)), while the shoulder and the satellite indicate the presence of $Cu(OH)_2$ and/or CuO. After sputtering, the lack of the peaks at 942 eV and 935 eV show that the sputtered spot only contains Cu_2O (or Cu(0)). The Cu_{LMM} signal (c) shows a peak 570 eV for the unsputtered surface (red) and 568 eV for the sputtered surface (green). These binding energies must be translated to the corresponding Auger kinetic energies and plotted against the Cu2p binding energies to differentiate between pure copper and cuprous oxide (i.e. Wagner plot).This Wagner plot, shown in Figure 20, indicates a presence of Cu_2O alongside the already measured CuO before sputtering and pure copper after sputtering.[30]

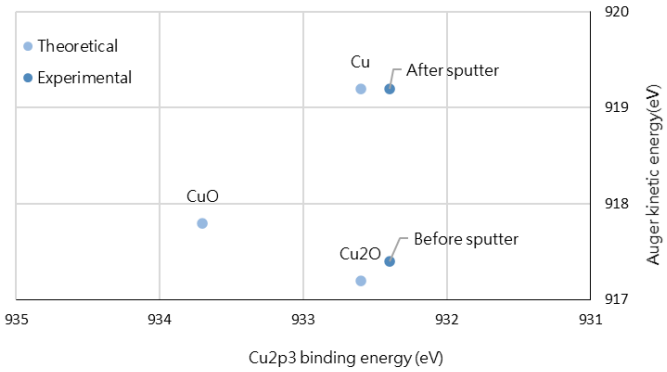

Figure 20: Wagner plot for model copper (from Goodfellow Inc.) for the theoretical values (light blue) and the experimental values (dark blue).

The atomic concentrations before and after sputtering are reported in Table 5. It shows the presence of a large amount of carbon, even deeper into the sample, as the C/O ratio is equal to 1,2 after 1 min. of sputtering, compared to 1,6 before sputtering.

Table 5: Atomic concentrations (%) of components in model copper

Before/After Sputter	Sputter depth (nm)	C (%)	O (%)	Cu (%)
Before sputtering	0	57	36	8
After sputtering (1 min.)	3,5	30	25	45

The oxide thus respectively consists of pure copper, a layer of Cu_2O and a top layer of CuO and $Cu(OH)_2$. Due to the calculation of the OH-fraction, we saw that the number of hydroxyl groups on the surface is relatively high, which might influence the adhesion mechanism as shown in literature. Surface contamination is present and remains present, although in smaller amounts, deeper into the sample.

5.1.1.2. Examination of the oxide layer of the copper from Myanmar

The copper from Myanmar was analyzed in an analogue way to the model copper provided by Goodfellow Inc. using XPS. High-resolution spectra were recorded for the elements that are present in the oxide layer (O1s, C1s, Cu2p and CuLMM). The sample was sputtered using a monoatomic argon source (specifications are equal to those in the previous section). The sample was sputtered for one minute. The sputter rate is assumed to be similar to that of SiO_2 (3,5 nm/s), meaning that the depth of the measurement after sputtering for one minute is equal to 3,5 nm.

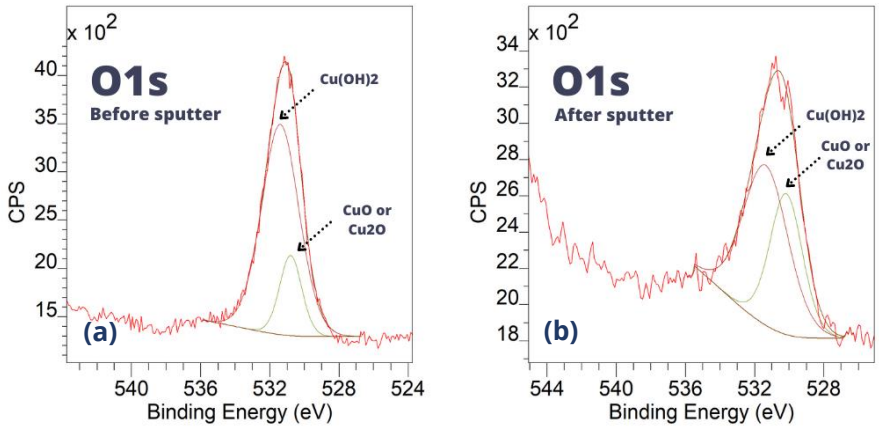

Figure 21: High-resolution XPS spectra of the O1s peak measured on copper from Myanmar (a) before sputtering and (b) after one minute of sputtering. The different contributions are illustrated by the deconvolution of the peak in a contribution at 532 eV ($CuOH)_2$ and 530 eV (CuO or Cu_2O).

Figure 21 shows the high-resolution XPS O1s peaks (a) before and (b) after sputtering. The O1s peak can again be deconvoluted into two peaks, a copper hydroxide contribution and a contribution that indicates the presence of oxides (cupric oxide and cuprous oxides cannot be distinguished here). Before sputtering (a), the contribution of the copper hydroxides to the peak seams larger than after sputtering (b). The hydroxyl fraction calculated from the atomic weight percentages of O-C=O, C-C-O, OH and O^{2-} is 11% before sputtering and 7% after sputtering. The remaining hydroxides probably originated in during the growth of the native oxide layer as copper hydroxides were formed and subsequently encapsulated by other oxide species. The peak decompositions are shown in Annex 9.2.

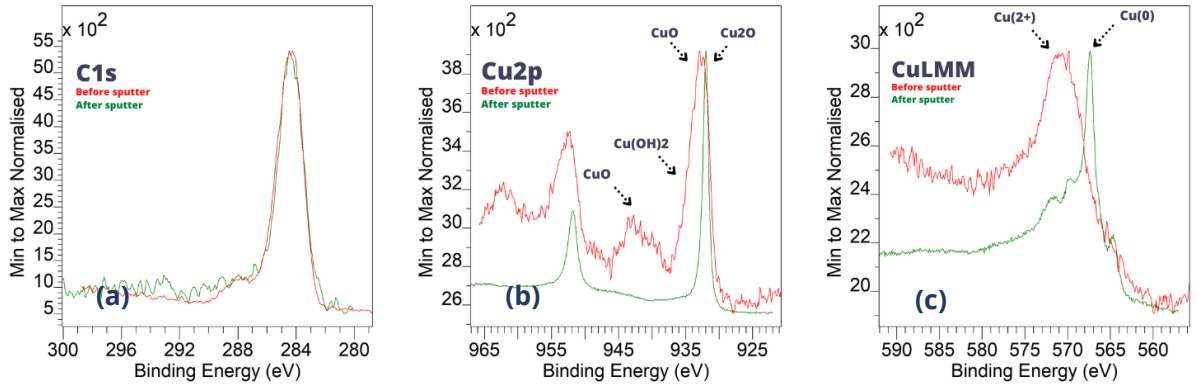

Figure 22: High-resolution XPS spectra of the (a) C1s peak, (b) Cu2p peak and (c) CuLMM peak for the copper from Myanmar. The sample was sputtered for one minute, the red spectra refer to the sample before sputtering and the green spectra to the sample after sputtering.

Figure 22 shows the high-resolution measurements of the C1s, Cu2p and CuLMM peaks (minimum to maximum normalized). The C1s peak (a) does not become noisier after sputtering like in the case of the model copper (see), which indicates a large contamination deep into the material. Cu2p peak (b) shows a signifying peak at 932 eV after sputtering (green) and an additional peak shoulder at 935 eV accompanied by a satellite peak at 942 eV before sputtering (red). This indicates the presence of only Cu_2O phases or Cu(0) after sputtering, while the top layer also contains CuO and $Cu(OH)_2$. The Cu_{LMM} signal shows the presence of a peak at 570,2 eV before sputtering (i.e. Cu2+)and 567,9 eV after sputtering (i.e. Cu(0)). To better understand the true nature of the oxides, these values must be plotted in a Wagner plot, as shown in Figure 23. This indicates that before sputtering, Cu_2O is present alongside the CuO, while pure copper is measured after sputtering.

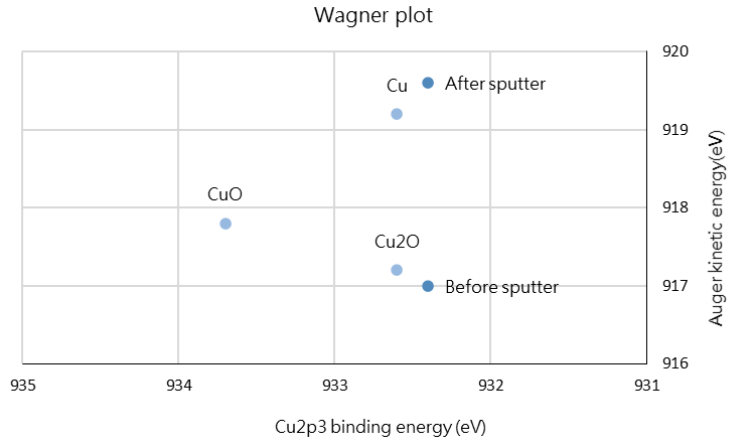

Figure 23: Wagner plot for copper from Myanmar for the theoretical values (light blue) and the experimental values (dark blue).

Table 6 shows that the contamination is much higher in this sample even deeper into the material, as the C/O ratio is equal to 2,2 even after 1 min. of sputtering, compared to 2,4 before sputtering.

Table 6: Atomic concentrations (%) of components in copper from Myanmar

Before/After Sputter	Sputter depth (nm)	C (%)	O (%)	Cu (%)
Before sputtering	0	67	27	5
After sputtering (1 min.)	3,5	28	13	59

The copper as received from Myanmar shows the same build-up as seen in literature[26,37,99] and on the model samples (see section 5.1.1.1.). They contain, however, a lower hydroxyl fraction on the surface and a larger carbon content. The model samples can thus be used as a reference, but caution must be taken when transferring obtained knowledge to the in situ application of the glue.

5.1.2. Study of the surface of different gold samples

The gold must be characterized in order to make sure it is not contaminated with other elements, as this can have an influence on the interfacial interactions. This is done for both the model gold used for adhesion tests (which is a gold deposited on mica glass and a gold electrode) and the

gold received from Myanmar. This will allow us to verify whether these model samples are a good reference for the gold from the pagoda.

5.1.2.1. Examination of the surface of gold leaf on mica glass

For the tests performed with DETA and succinic acid, a gold layer deposited on mica is used. This gold will be analyzed using high-resolution XPS spectra of the elements that were present (C1s, O1s and Au4f) and sputtered to better understand the depth of the contamination layer on this gold. The sputtering was performed for one minute using a sputter rate of 3kV (6 nm/min for SiO_2). The sputter rate ratio between gold and SiO_2 is equal to 4,8 meaning that the sputter depth after one minute of sputtering is equal to 29 nm.[29]

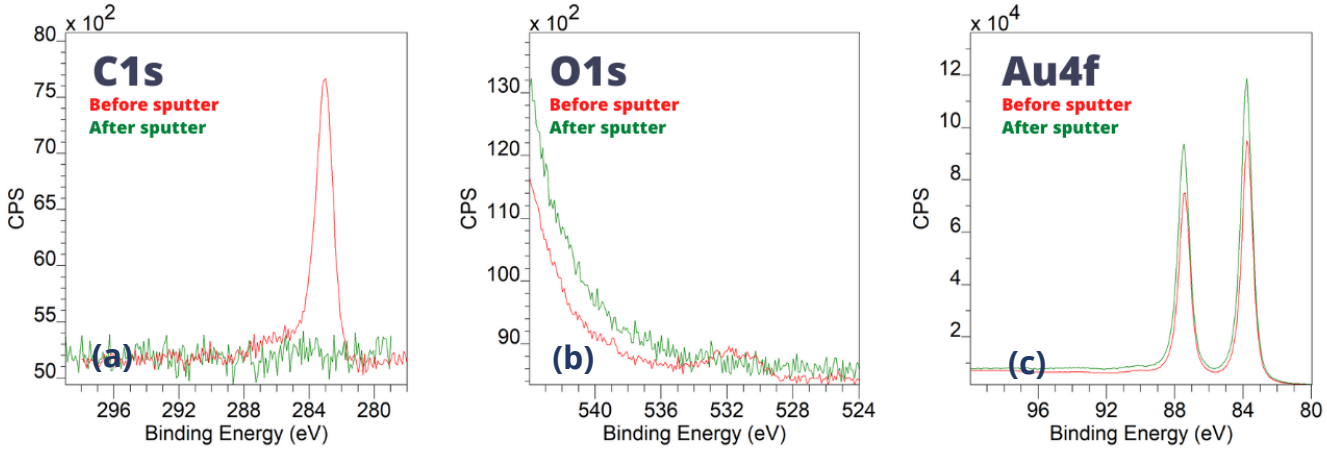

Figure 24: High-resolution XPS spectra of the (a) C1s peak, (b) O1s peak and (c) Au4f peak for the gold deposited on mica. The sample was sputtered for one minute, the red spectra refer to the sample before sputtering and the green spectra to the sample after sputtering.

Figure 24 shows the high-resolution XPS spectra for the model gold that will be used to analyze the reactions with DETA and succinic acid. The C1s peak (a) disappears entirely after one minute of sputtering, which illustrates that the small contamination layer on the gold. The O1s peak (b) is almost non-existent before and after sputtering, which illustrates the limited amount of organic contamination. The gold leaf on mica glass is thus clearly pure gold, which can be seen in the clear Au4f (c) peaks. Because of the low O1s peak and the disappearing C1s peak, it can be concluded that the gold contains a carbon and oxygen contamination layer, which is removed after sputtering.

Table 7 confirms this, as the atomic percentage of carbon goes from 35% to 0%, whereas the atomic percent of gold is equal to 100% after sputtering.

Table 7: Atomic concentrations (%) of components in gold on mica

Before/After Sputter	Sputter depth (µm)	C (%)	O (%)	Au (%)
Before sputter	0	35	1	64
After sputter (1 min.)	1	0	0	100

5.1.2.2. Examination of the gold surface on the gold electrode

The gold electrode will be used for the thiol submersion tests, to limit the amount of material waste and cost. Indeed, the electrode will be repolished in between submersion tests and used for all thiol tests. It is therefore again important to elucidate composition of the surface and the contamination that is present. High-resolution spectra of the elements that are present (O1s, C1s and Au4f) were recorded.

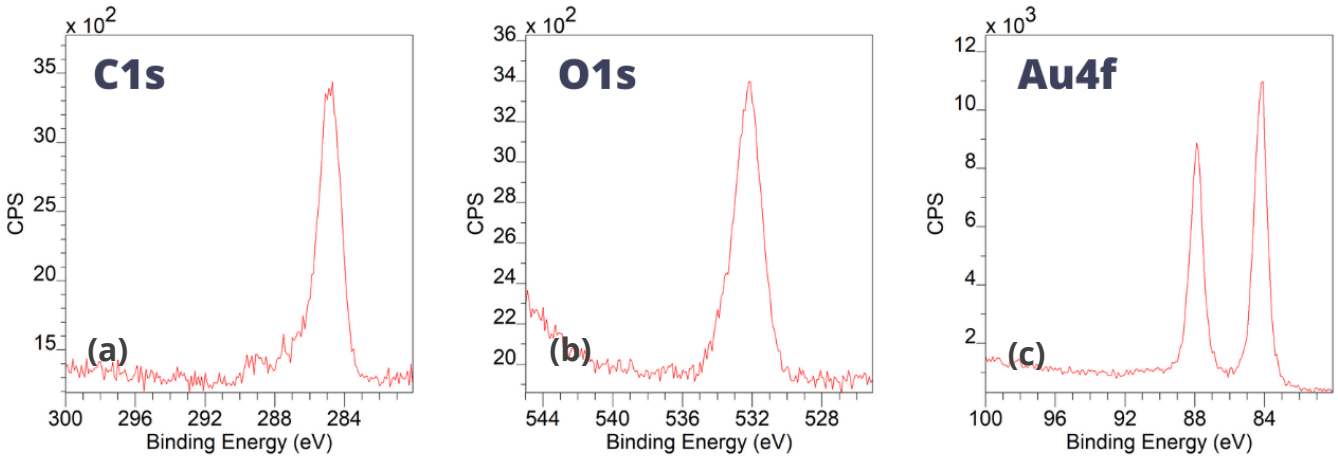

Figure 25: High-resolution XPS spectra of the (a) C1s peak, (b) O1s peak and (c) Au4f peak for the gold electrode after a polishing step and a cleaning step with organic solvents.

Figure 25 shows the XPS high-resolution spectra acquired on the gold electrode. The measured C1s (a) and O1s (b) peak illustrate the presence of organic contamination (as seen before, the gold is not oxidized at the surface). The Au4f (c) peak shows that the gold electrode is made of pure gold. Table 8 confirms this C/Au ratio is equal to 4,2 and the C/O ratio is equal to 3,3.

Table 8: Atomic concentrations (%) of components in gold electrode

Sample	C (%)	O (%)	Au (%)
Gold electrode	65	20	15

5.1.2.3. Examination of the surface of the gold used on the pagoda

The gold that was received from Myanmar should also be analyzed to verify the validity of the use of the model gold (both the gold deposited on mica and the gold electrode). This gold was rolled in Myanmar, in a factory next to the site and examined as received. This analysis will be performed using high-resolution XPS spectra of the occurring elements (C1s, O1s and Au4f) and by sputtering the sample for twelve minutes using a sputter rate of 3 kV. This corresponds to a depth of about 350 nm. During sputtering no high-resolution spectra were recorded, only the relative amount of Au4f compared to C1s was determined, as reported in Figure 27.

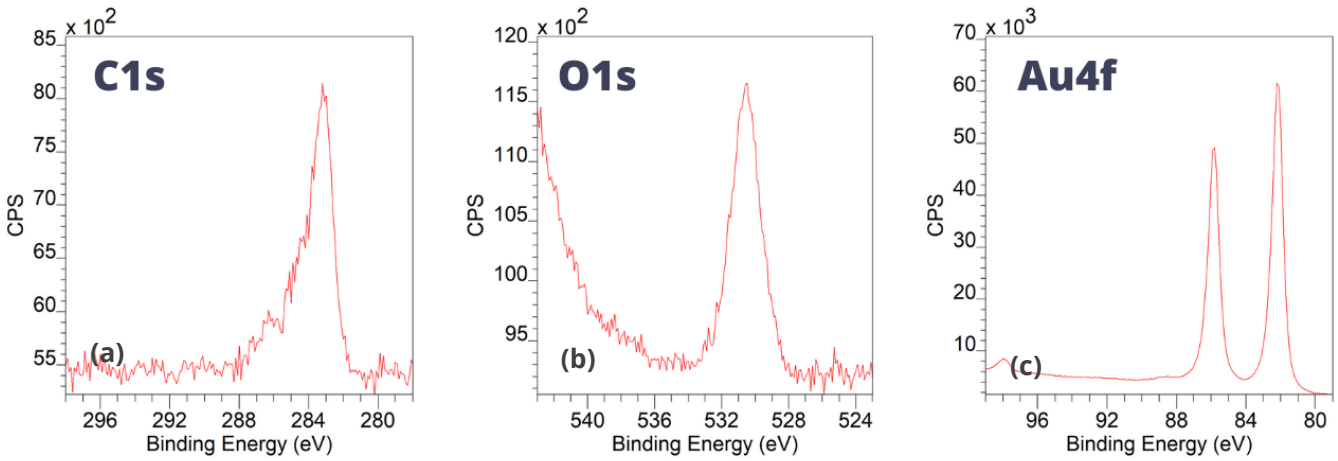

Figure 26: High-resolution XPS spectra of the (a) C1s peak, (b) O1s peak and (c) Au4f peak for the gold from Myanmar

Figure 26 shows the high-resolution XPS peaks measured on the gold received from Myanmar. The C1s peak (a) and O1s peak (b) indicate the presence organic contamination. The gold from Myanmar is clearly pure gold, which can be seen by the Au4f peak. It does, however, contain a significant carbon and oxygen contamination layer, which is not totally removed after a severe sputtering of 348 nm (corresponding to a sputter time of 12 minutes), as can be seen in Figure 27.

Table 9: Atomic concentrations (%) of components in gold from Myanmar before sputtering

Before/After Sputter	Sputter depth ((µm)	C (%)	O (%)	Au (%)
Before sputter	0	48	16	36
After sputter (12 min.)	12	22	8	71

The samples from Myanmar seem to have a similar surface to the model samples from the VUB, although they contain a larger contamination layer, as can be seen in Table 9 and Figure 27. Table 9 shows the atomic concentrations and allows to deduce that the C/Au ratio after sputtering is still equal to 0,3 compared to 1,3 before sputtering. This can be explained by the rolling process used for gold. Gold is rolled using oils which can cause a large amount of organic contamination, deep into the material. The VUB samples can thus be used as a reference, but caution must be taken regarding the possible effects of the high amount of contamination for actual application.

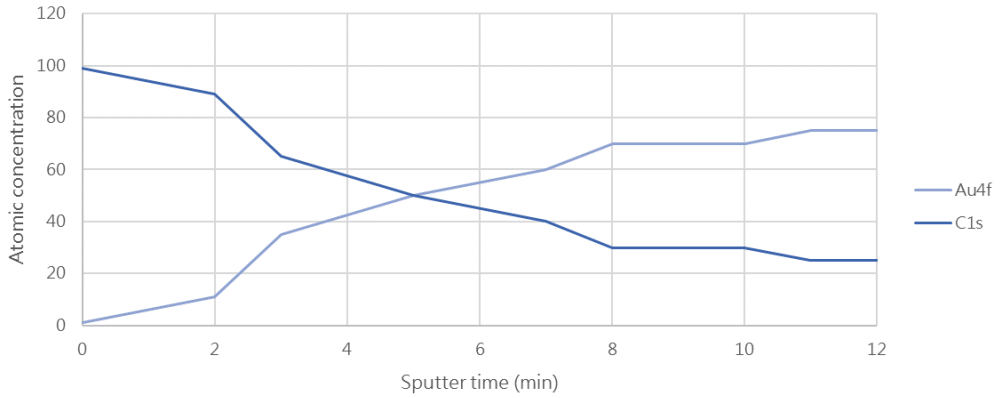

Figure 27: Relative contributions of the C1s and Au4f peak during the sputter profile of gold from Myanmar

5.2. What interactions occur between the surface of metals and organic material in model systems?

Once the samples are characterized, the interactions with different model molecules can be evaluated. Three different model molecules will be used (i) diethylenetriamine or DETA to mimic the glue that is currently used on the temple in Myanmar, (ii) succinic acid to mimic natural oils that are traditionally used for gluing gold leaf[63] and (iii) thiols because of their proven interaction with both gold and copper in literature.[61,81]

5.2.1. Microscopic analysis of the cross section of the glued material

A preliminary analysis using optical microscopy, as shown in Figure 28, showed a layered structured composed of copper (brown, top), glue (black) and gold (brown, bottom). Since contact with Myanmar was lost during the coup d'état, there is no explanation for the use of this top layer.

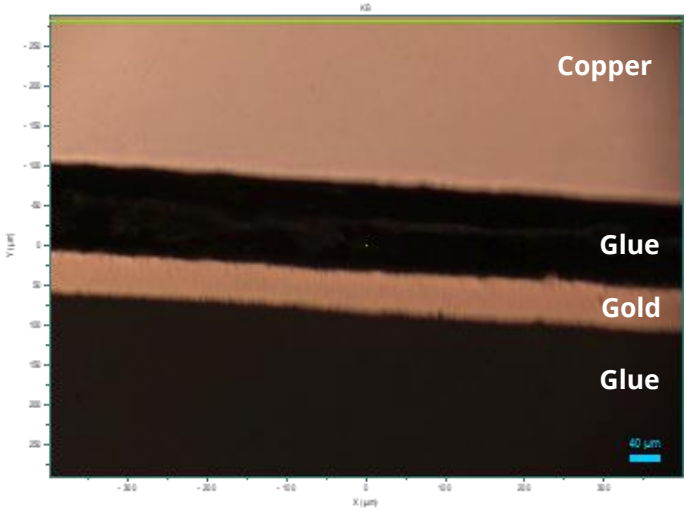

Figure 28: Microscopic image of the cross section of the received, unused glued sample, with copper (top), glue (black) and gold (bottom).

The result is that the gold is embedded in a glue layer instead of being glued on the copper. The same glue top layer can be seen in systems that use gold leaf, although this is probably caused by the glue that diffuses through small pores of the gold leaf.

This image can explain the adhesion of gold onto the glue and thus the copper, as it is embedded, and therefore not automatically physically or chemically adhered. If the glue layer gets damaged, the durability of the interface will depend on the chemical and physical interaction at play between the gold and the glue.

5.2.2. Interactions of the metals with amines

The interaction with amines is studied to mimic the chemical interaction with the glue currently used on the temple and provided by Huntsman. Both gold and copper will be submerged in a 0,1 wt.% DETA solution for 30 minutes.

5.2.2.1. Characterization of the interaction of gold with DETA

After submersion of the gold deposited on mica in DETA, the sample was analyzed using XPS and a high-resolution measurement of the C1s, O1s, Au4f and N1s peak was performed. The N1s peak will allow to investigate the type of interaction between gold and DETA. The other peaks are used to determine the relative atomic concentrations, which can be used to determine the N/Au ratio and the N/C ratio. The N/Au ratio gives an idea of the coverage of the sample (the higher this number, the larger the number of species that were adsorbed) and the N/C ratio can indicate the amount of carbon contamination remaining on the sample, as it will be compared to the stoichiometric ratio. If the N/C ratio is lower than the stoichiometric ratio of DETA, some carbon species that do not originate from DETA will be observed.

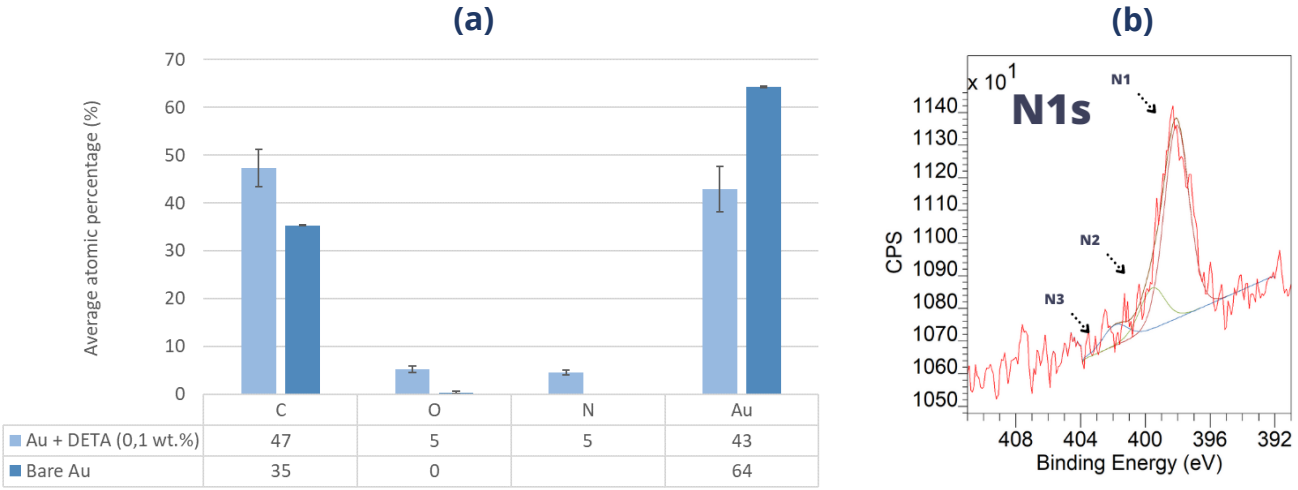

Figure 29: Average atomic concentrations (a) and high-resolution XPS signal of the N1s peak (b) from gold submerged in DETA (0,1 wt.%) for 30 minutes, fitted using the procedure explained in section 4.3.1.1.

In Figure 29 (b) the N1s peak is fitted to evaluate the contributions of the N1 species (physically adsorbed species or weak Lewis acid-base interaction), the N2 species (Lewis-acid interactions)

and N3 species (Bronsted acid-base interactions or ionic interactions). The binding energy (BE) is equal to 398 eV and the FWHM is equal to 1,6 for all species. Only a significant amount of the N1 species is observed, which illustrates the weak interaction between copper and gold. Figure 29 (a) allows to evaluate the contribution of the different elements to the measured spectrum. The N/C ratio (0,1) is much lower than the stoichiometric ratio of DETA (0,75). The N/Au ratio (0,1) is much lower than the N/Cu (2,9) ratio that will be reported in the next spectrum. Some DETA molecules thus adhered on the surface, but the amount is rather low. The Au/C ratio for the submerged sample (0,9) is lower than the Au/C ratio for the bare substrate, showing a sort of cleaning effect from this treatment. Some carbon was removed, but even more was replenished due to the adsorption of DETA. This cleaning effect was already perceived an confirmed by other researchers, as discussed by Pletincx et al.[100]

5.2.2.2. Characterization of the interaction of copper with DETA

The model copper samples will be submersed in a 0,1 wt.% DETA solution. The interaction between DETA and copper will be confirmed using ToF-SIMS and the mechanism is further studied using an increased concentration of DETA solution.

5.2.2.2.1. Copper submersion in 0,1 wt.% DETA

The treated sample was analyzed using XPS and a high-resolution measurement of the C1s, O1s, Cu2p and N1s peak was performed. The N1s peak will allow to investigate the type of interaction between copper and DETA by performing a peak fitting as shown in the previous section. The relative atomic concentrations were determined using the information from all peaks. The N/Cu ratio will be used to determine the amount of DETA species adsorbed and the N/C ratio will be compared with the stoichiometric ratio to evaluate the contamination. Three different samples will be compared

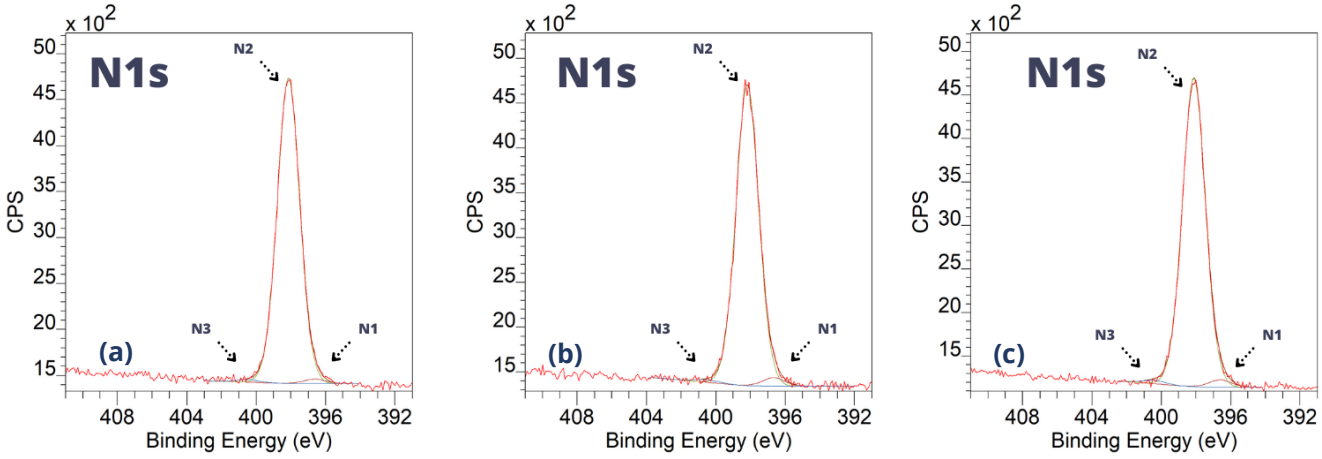

Figure 30: High-resolution XPS signal of the N1s peak form copper submerged in DETA (0,1 wt.%) for 30 minutes for (a) a first sample, (b) a second sample and (c) a third sample. The peaks were fitted using the deconvolution as described in section 4.3.1.1.

The high-resolution N1s peak for all these samples is shown in Figure 30. The decomposition clearly indicates the main presence of an N2 peak. The ratio of the N2/N peak is equal to no less than 98% for all cases. However, since the N1 and N3 contributions are rather low, performing a

correct relative peak fitting is difficult, as at least one shoulder is normally used as a reference for the positioning of the other peaks. To confirm that the major contribution in this signal is indeed the N2 peak, a characterization using ToF-SIMS will be performed.

Table 10: Atomic concentrations (%) of components in copper treated with DETA (0,1 wt.%)

Bare copper			
C	O	N	Cu
62	24	0,4	13
Copper + DETA (0,1 wt.%)			
C	O	N	Cu
56	17	19	7

The stoichiometric ratio of N/C in the DETA molecule (0,75) is more than double the measured N/C value for the Cu + DETA measurements (0,3) as can be derived from Table 10, indicating that not all carbon contamination was replaced by DETA. Table 10 reports the average value for the measured samples. The high N/Cu ratio (2,9) indicates the high amount of DETA molecules that were adsorbed.

5.2.2.2.2. ToF-SIMS on copper submerged in DETA (0,1wt%)

ToF-SIMS measurements will be performed to verify the formation of a copper-DETA complex and thus a strong interaction (i.e. chemisorption) between the substrate and the model molecule.

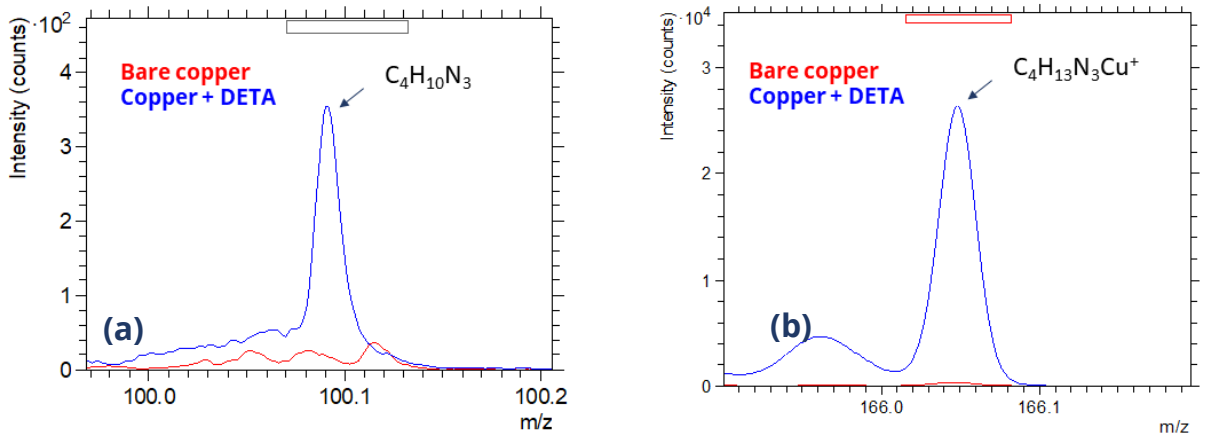

Figure 31: SIMS intensity for (a) $C_4H_{10}N_3$ species and (b) $C_4H_{13}N_3Cu^+$ species or $[Cu + MDETA]^+$ for bare copper (red) and copper + DETA 0,1 wt.% (blue) for 30 minutes.

In the SIMS data (Figure 31) the bare substrate (red) is compared to the copper after submersion in DETA (blue). These positive ion mass spectra show the presence of both DETA characteristic fragments such as $C_4H_{10}N_3^+$ at *m/z* 100 (DETA chemical formula is $C_4H_{13}N_3$) (left) and copper-DETA complexes like $C_4H_{13}N_3Cu^+$ or $[Cu + M_{DETA}]^+$ at *m/z* 166 (right). The presence of the latter fragment ion (containing one Cu atom) is confirmed by the isotopic ratio of the copper atoms (^{63}Cu and ^{65}Cu) found between the peaks at *m/z* 166 and 168. This ratio of $^{63}Cu/^{65}Cu$ is equal to 2,4.[101] The

ion $C_4H_{13}N_3Cu^+$ is proving the chemical interaction between the Cu atoms on the substrate and the amine groups of the model molecule.

The measurement of a Cu-N component shows the strong interaction between the substrate and the model molecules and allows to conclude that the major contribution is indeed an N2 contribution indicating a Lewis-type interaction. This information, together with the high N2/N1 ratio allows to say that there are multiple strong bonds formed between one DETA molecule (containing three sites, the amine groups) and the substrate.[18] This will, however, be different in case of the use of glue, as the sterical hindrance will impede multiple bonds from being formed.

In order to better understand the mechanism behind this interaction, however, more information on the different contributions is required. Therefore, the DETA concentration will be increased to see the effect on the different contributions of the N1s peak.

5.2.2.2.3. Copper submerged in DETA with a higher concentration

The peak fitting based on relative positions is possible in the presence of at least two peaks. Therefore, the aim is to make sure that the sample contains both an N2 (Lewis-type interaction) and N1 (non-interacting amine nitrogen or weak Lewis-type acid-base interaction) contribution.[93] The concentration of the DETA will be increased to observe the effect on the N1 contribution to the N1s peak. This concentration can, however, not be too high not to imperil the vacuum in the VersaProbe II. Therefore, IR-spectroscopy measurements were performed for different concentrations (0,3 wt.%, 0,4 wt.% and 1 wt.%) to find the lowest concentrations at which the physically adsorbed species are still present.

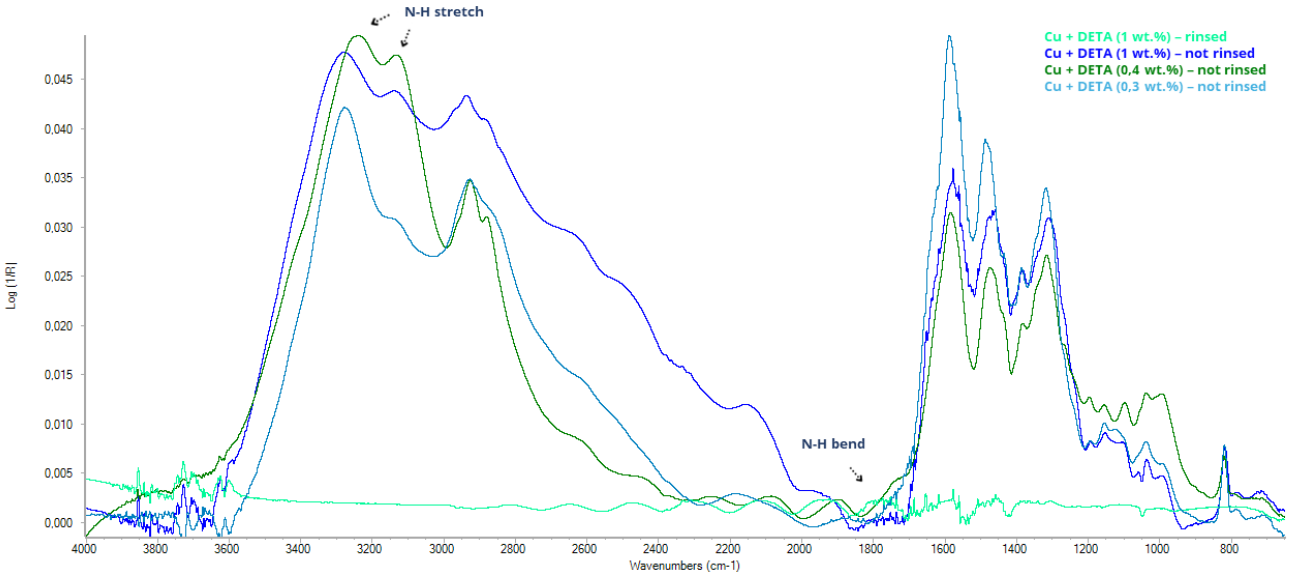

Figure 32: IR spectroscopy of copper submerged in DETA for different concentrations: 0,3 wt.% of DETA not rinsed with THF (light blue), 0,4 wt.% of DETA not rinsed with THF (dark green), 1 wt.% of DETA not rinsed with THF (dark blue) and 1 wt.% of DETA rinsed with THF (light green).

In Figure 32 the IR spectra of samples treated with different concentrations of DETA are shown. The red spectrum was observed for a submersion in a concentration of 1 wt.% DETA after which

the sample was rinsed. This spectrum shows no signifying peaks, which is caused by the thin DETA layer, much thinner than the depth resolution of the IR beam (µm size). DETA unvails signature peaks at both 3300 cm^{-1}, 3100 cm^{-1} and 1900 cm^{-1} as seen for the non-rinsed sample. This indicates a thick layer of DETA, comparable to the depth resolution of the IR spectrometer (µm size). Because of the thickness of this layer, physically adsorbed species are known to be present. For a concentration of 0,4 wt.% tthe same peaks are observed, while the intensity starts to lower for 0,3 wt.%. Therefore, a concentration of 0,4 wt% was used for the upcoming measurements.

The IR spectroscopy clearly showed a difference between the rinsed and non-rinsed samples. The low intensity for the rinsed case could be caused by the fact that only chemically adsorbed species remain and form a thin, strongly adhered layer on the surface. To evaluate the effect on the interactions, the samples were characterized using high-resolution XPS measurements of the N1s peak.

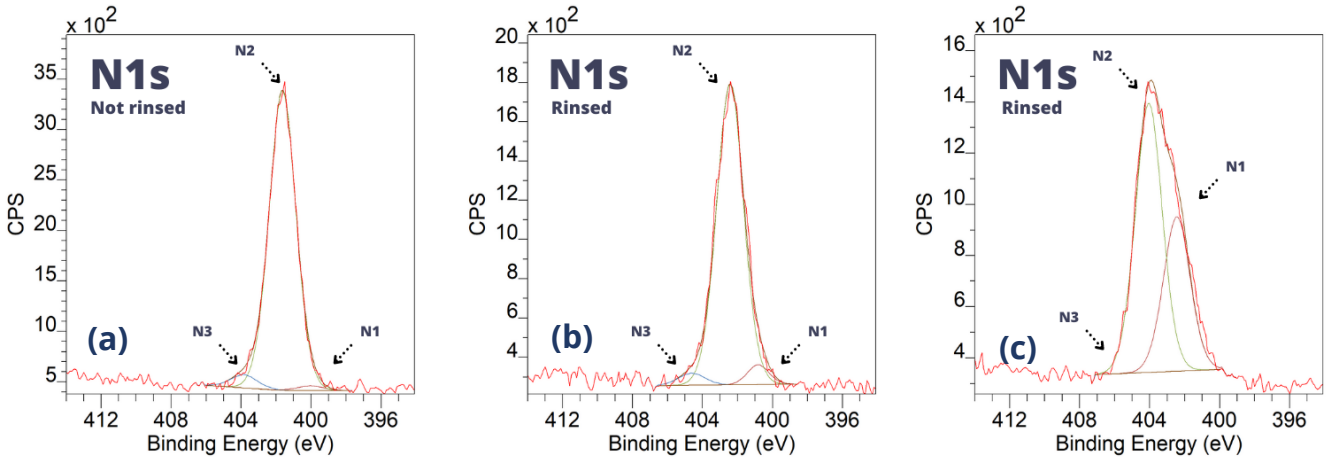

Figure 33: A comparison of the high-resolution XPS signal of the N1s peak for (a) the not rinsed case and (b) a first point and (c) second point on the rinsed sample of copper submersed in 0,4 wt% DETA for 30 minutes. The peaks were fitted using the deconvolution described in section 4.3.1.1.

Figure 33 shows a large N2 contribution for all samples, (a), (b) and (c). The N1s peak of sample that was not rinsed (a) has only very small N1 and N3 contributions, while the rinsed sample shows already larger contributions (b) and even very large N1 contributions for some points (c). The surface that was not rinsed was homogeneous when it comes to the N1s contibutions, whereas the rinsed sample showed inhomogeneities (not all measuring points are shown in Figure 33).

Figure 34 allows to deduce that the N/Cu ratio is lower for the rinsed case (2,0) compared to the non-rinsed case (2,8). The higher this ratio, the more DETA that adheres on the surface, so more coverage is observed for the not rinsed case, which corresponds to the findings of the IR spectroscopy. The N/C ratio is around 0,3 for both measurements and is thus equal to that for the submersion in DETA of 0,1 wt.%. This is lower than the stoichiometric ratio of 0,75 which shows that some carbon doesn't originate from the DETA molecules. This illustrates the presence of DETA

and some residual surface contamination. To understand the type of interactions, the relative contributions of the N1, N2 and N3 species to the N1s peak must be analyzed.

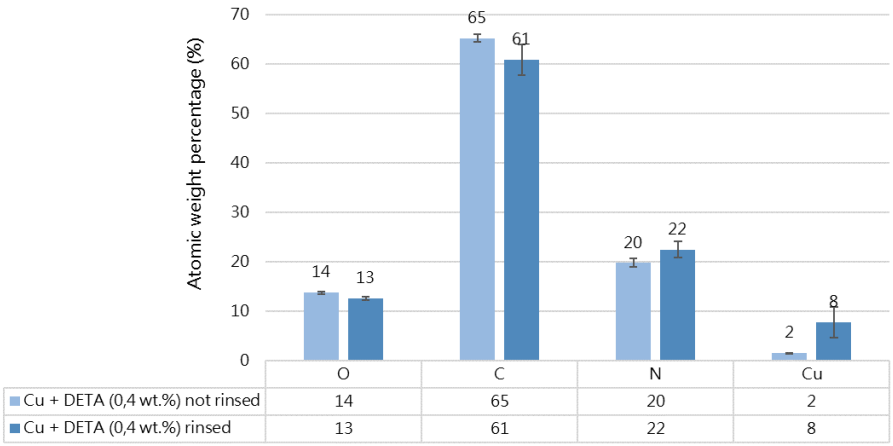

Figure 34: Atomic weight percentages of the N1s peak for the rinsed and non-rinsed samples of copper submerged in 0,4 wt.% DETA for 30 minutes. Rinsing is performed using the solvent, THF.

Figure 35 illustrates these relative contributions of the different nitrogen species. There is a large error found (seen in the error bars) on the N1 and N2 contributions for the rinsed case (dark blue), which illustrates the inhomogeneity. The N1 contribution is much higher for the rinsed case (dark blue).

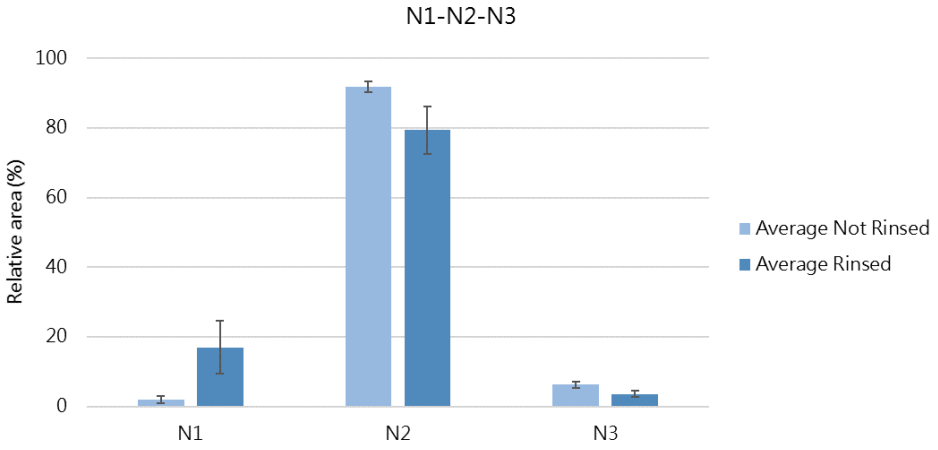

Figure 35: The relative contributions of N1, N2 and N3 species tot the N1s peak for copper submerged in DETA (0,4 wt.%) for 30 minutes for the not rinsed (light blue) case and the rinsed case (dark blue), where the samples was rinsed with the solvent (THF).

The large N1 contribution for the rinsed case is unexpected, as rinsing was supposed to remove the physically adsorbed species. The IR spectroscopy showed that the samples that were not rinsed contain a thicker layer of DETA molecules, while the XPS measurements define this top layer as being N2 species and thus chemically interacted species. It is difficult to say what causes this phenomenon, as there are many possibilities, such as a difference in spatial resolution for the IR spectroscopy and the XPS measurement or a specific interaction such as enhanced wet adhesion

as described by Pletincx et. al.[94] In this enhanced wet adhesion, as described for aluminium oxides and PAA, a carboxylate anion is formed due to interaction with water which can in turn form a complex with aluminium. An analogue mechanism could occur for rinsing if THF is able to deprotonate the DETA. This is, however, only a hypothesis and should be confirmed using a complementary in situ technique such as IR in Kretschmann configuration which would allow to learn more about the in-depth distribution of species. ToF-SIMS could also allow to learn more about the formed complexes.

5.2.3. Interactions components based on natural oils

To mimic the functional groups that are present in natural oils, succinic acid (SA) is used as a model molecule and both copper and gold samples will be submerged for 30 minutes. This investigation will allow to form an idea on the chemical bond formation of the substrates with the historically used natural oils.

5.2.3.1. Gold submersion in 0,1 wt.% succinic acid

The gold deposited on mica will be submerged in a 0,1 wt.% SA and high-resolution spectra of the C1s, O1s and Au4f peaks will be measured. These peaks will be used to evaluate the atomic weight percentages of the elements present on the top layer. The C/Au ratio after submersion can be compared to that of the bare substrate. The amount of carbon on the surface must be treated with care, however, as it can be an indication of the adsorbed succinic acid or surface contamination. That is why the C/O ratio must also be evaluated and compared to the stoichiometric ratio of SA (which is equal to 1). The C1s peak will be decomposed into several contributions as described in section 4.3.1.1 and suggested by Pletincx et al.[94] in order to evaluate the relative amount of COO^- and COOH species. The contribution of these species and their relative ratio ($[COO^-]/[COO^-]+[COOH]$) can be used to evaluate the amount of interactive species as proposed by Pletincx et al.[100] The higher this ratio, the more interaction between the carboxylic acids and the substrate will occur.

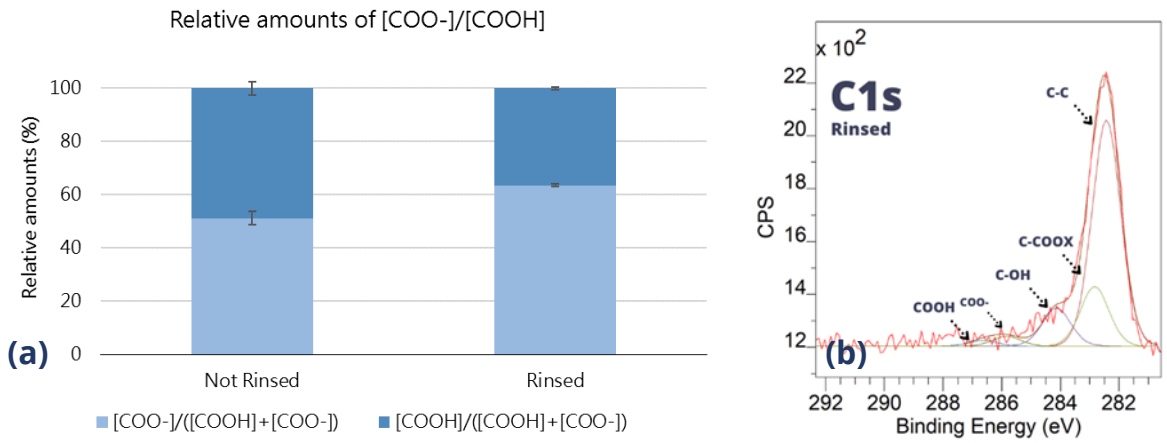

Figure 36: Atomic weight percentages of the O, S and Au elements (a) and relative contributions to the C1s peak (b) for gold submerged in 0,1 wt.% succinic acid for 30 minutes, rinsed (dark blue) and not rinsed (light blue) using the solvent (THF).

Figure 36 shows the atomic weight percentages for the different components of the Au + SA spectrum and the relative contributions of the different carbon containing species to the C1s peak. The Au/C ratio, which can be deduced from the atomic weight percentages in Figure 36 (a), is a higher for both the rinsed for the not rinsed case (0,93 on average) than it was for the bare substrate (0,55). This indicates an increased amount of carbonate species. The C/O ratio, however, is much higher (15,3) than the stoichiometric ratio (1,0). This illustrates that not all carbon containing species originate from SA. There is not really a difference between the rinsed and non-rinsed case when it comes to atomic weight percentages. Figure 36 (b) illustrates the contributions to the C1s peak, where it can be seen that the relative amounts of both COOH and COO^- are low for both the rinsed and the not rinsed case.

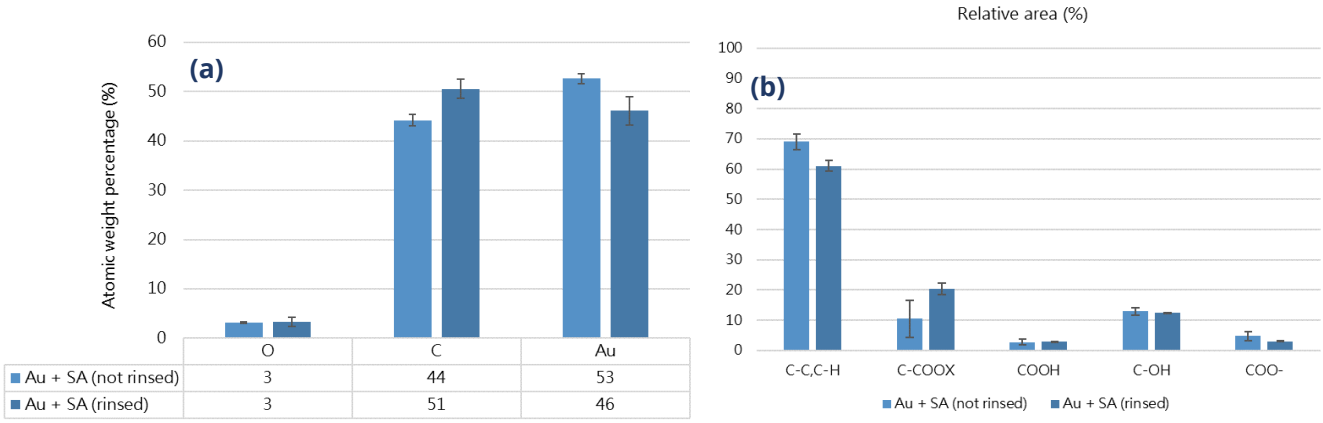

Figure 37: (a) Relative amount of carboxylates (light blue) and carboxylic acid (dark blue) for gold submergea in 0,1 wt.% succinic acid for 30 minutes for a non-rinsed (left) and rinsed (right) sample and (b) example of the peak deconvolution of the C1s peak for the rinsed sample, as described in section 4.3.1.1.

Figure 37 illustrates the relative amount of COO- species compared to the COOH species, which gives an idea whether the material interacted or not. It shows that the amount of COO^- species (light blue) is rather high compared to the COOH (dark blue) species. Although this relative amount is rather high, the absolute amount is rather low as shown in Figure 36 and C/O ratio doesn't approach the stoichiometric ratio of SA. Thus, an interaction is observed between the gold substrate and the succinic acid, but the amount seems rather low. As carboxylate species are formed, the strength of this interaction is ionic, giving rise to properties as illustrated in Table 1.[94] It is important to note that the decomposition of the peaks in the shoulder area, as shown in Figure 37 (b) might contain some errors due to its low intensity, which can give rise to a false interpretation of the results. Further investigation is required.

In further tests, the importance of time for the self-assembly of components of gold was illustrated. In order to be able to exclude the possibility of strong interaction of these compounds with gold, longer submersion times should be evaluated.

5.2.3.2. Copper submersion in 0,1 wt.% succinic acid

Copper is analyzed in an analogue way and is submerged in 0,1 wt.% succinic acid for 30 minutes and high-resolution spectra of the C1s, O1s and Cu2p peaks were measured. These are used to determine the atomic weight percentages of the elements present in the samples and to

determine the C/Cu and C/O ratio which allow to evaluate the number of adhered species. The C1s peak is decomposed, as suggested by Pletincx et al. and described in section 4.3.1.1.[94] This allows to evaluate the relative contributions of carboxylate species to the spectrum and also determine the ratio of carboxylates to carboxylic acids in order to evaluate the number of interacted species.

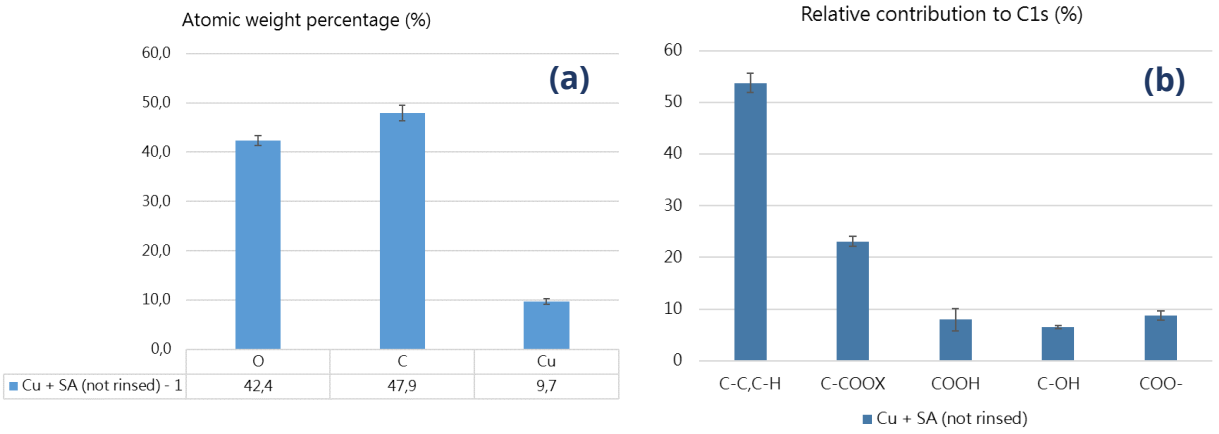

Figure 38: (a) Atomic weight percentages of the O, C and Cu elements and (b) relative contributions of the C1s peak for non-rinsed samples of copper after submersion in 0,1 wt.% of succinic acid for 30 min.

Figure 38 (a) allows to deduce that the C/Cu ratio is much higher for the submerged sample (4,8) than it was for the bare substrate (1,4). The C/O ratio (1,1) approximates the stoichiometric ratio of SA (1,0) indicating the presence of SA species on the substrate. Figure 38 (b) shows that the relative amount of carboxylate species is about three times as high compared to the gold substrate. Figure 39 (b) confirms the increased presence of carboxylate species, by showing a signifying peak around 288 eV. This allows for a peak decomposition with a higher degree of certainty. Figure 39 (a) indicates the relative amount of carboxylate species compared to carboxylic acid, which is about 50%, and illustrates a good interaction between the copper substrate and the succinic acid. This can be caused by a counteracting adhesion reaction and 'cleaning effect', as the succinic acid is adsorbed, and the surface contamination is removed. The strength of the interaction is ionic, giving rise to properties as illustrated in Table 1.[94]

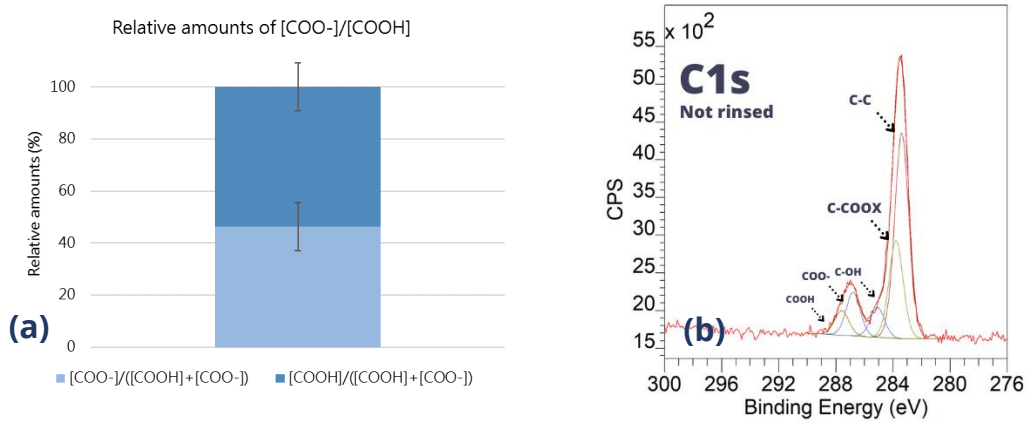

Figure 39: (a) Relative amount of carboxylates (light blue) and carboxylic acid (dark blue) for copper submerged in 0,1 wt.% succinic acid for 30 minutes for a non-rinsed sample and (b) example of the peak deconvolution of the C1s peak for the non-rinsed sample, as described in section 4.3.1.1.

5.2.4. Interactions with thiols

The last model molecule that will be analyzed is 1-octanethiol. Both gold and copper were reported to interact with the molecule, making it an interesting candidate for adhesion testing.[60,61,72,73,77,78,80,81,102] The samples will be submerged for one hour and 24 hours respectively (as the self-assembly of gold is known to require a longer time span[72]). The samples will be characterized using XPS and high-resolution spectra of all elements present will be recorded. The atomic weight percentages will again be used to determine ratios of present elements to deduce the relative amount of thiols adsorbed on copper and gold. The focus will be the decomposition of the S2p peak, as this allows to differentiate between thiolates (interacted species) and unbound thiols.

5.2.4.1. Submersion of gold in 1-octanethiol (1mM)

The gold electrode was submerged in 1-octanethiol (1mM ethanolic solution) for one hour and 24 hours respectively. Figure 40 reports the high-resolution XPS spectra of the S2p peaks for (a) one hour and (b) 24 hours. The S2p peak was decomposed into a thiolate contribution at 162 eV and a contribution from the unbound thiols (163 eV) as described in section 4.3.1.1.

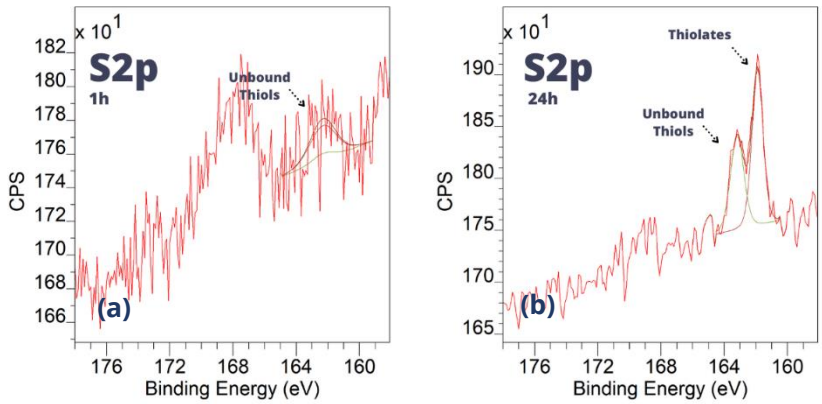

Figure 40: High-resolution XPS spectra of S2p for gold submerged in an ethanolic 1-octanethiol (1mM) solution for (a) 1 hour and (b) 24 hours. The peaks were decomposed as described in section 4.3.1.1. into a contribution from the unbound thiols at 163 eV and one from the thiolates at 162 eV.

Figure 40 (a) shows that there is almost no signal around 162 eV for the gold that was submerged for only one hour. Figure 40 (b) shows a clear two-component peak around 162 eV, with a higher contribution from the thiolates compared to the unbound thiols. This confirms the need for time when it comes to the self-assembly of thiols on the gold substrate.

Figure 41 shows the atomic weight percentages determined from the O1s, C1s, S2p and Au4f peaks for the gold submerged in the thiolic solution for one hour and 24 hours compared to the bare substrate. It allows to derive the S/Au ratio which gives an idea on the amount of adsorbed species. The S/Au ratio for the bare substrate and submersion for one hour are equal to 0, whereas the ratio for the 24 hour submersion is equal to 0,05 which corresponds to the values found in

literature.[80] The S/C ratio is, however, rather low (0,04) compared to the stoichiometric ratio of 1-octanethiol (0,13). Not all carbon species thus originate from the thiol molecule.

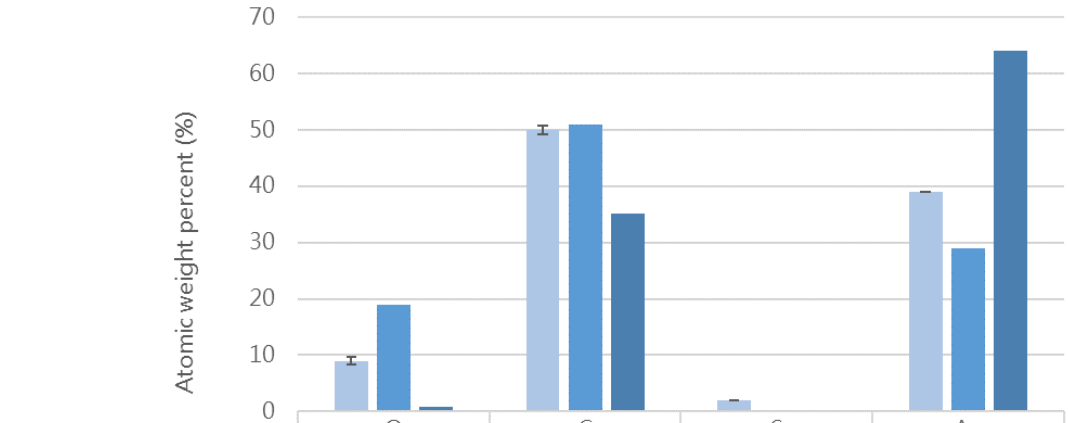

	O	C	S	Au
Au + 1-octanethiol (24h)	9	50	2	39
Au + 1-octanethiol (1h)	19	51	0	29
Bare Au	1	35	0	64

Figure 41: Atomic weight percentage for gold submerged in an ethanolic 1-octanethiol (1mM) solution for 1 hour, 24 hours and for the bare substrate

The relative number of thiolates compared to the unbound thiols can give an idea on the amount of interacted species and the average value and standard deviation for different gold samples is shown in Figure 42.

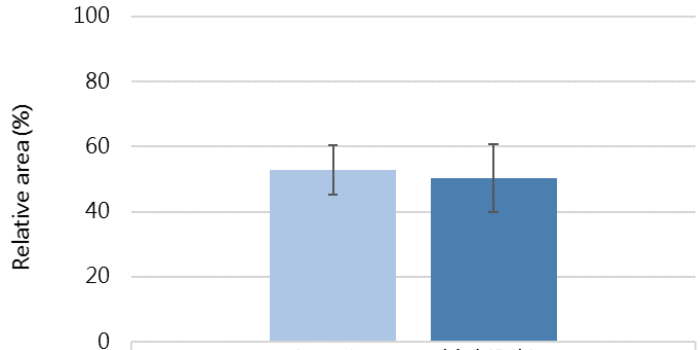

	Au + 1-octanethiol (24h)
Thiolate	53
Unbound thiol	50

Figure 42: Relative amount of thiolates and unbound thiols for gold submerged in 1mM 1-octanethiol

The large error bars in Figure 42 illustrate the inhomogeneous distribution of the thiolate species on the sample. In general, the number of thiolate species is rather high (53%) and this information, together with the previous statements allows to derive the fact that there is a good interaction between gold and thiols. In order to derive more information on the bond strength and mechanism, ToF-SIMS measurements can be used to define the formed complexes.

5.2.4.2. Submersion of copper in 1-octanethiol

In an analogue way copper was submerged in 1-octanethiol (1mM ethanolic solution) for one hour and 24 hours (Annex 10.3.). Some samples were rinsed with ethanol to evaluate the effect on unbound species. High-resolution spectra of the C1s, O1s, S2p and Au4f were recorded to evaluate the atomic weight percentages of each element. The high-resolution spectra of the S2p peaks were decomposed in a thiolate and unbound thiol contribution, as explained in section 4.3.1.1.

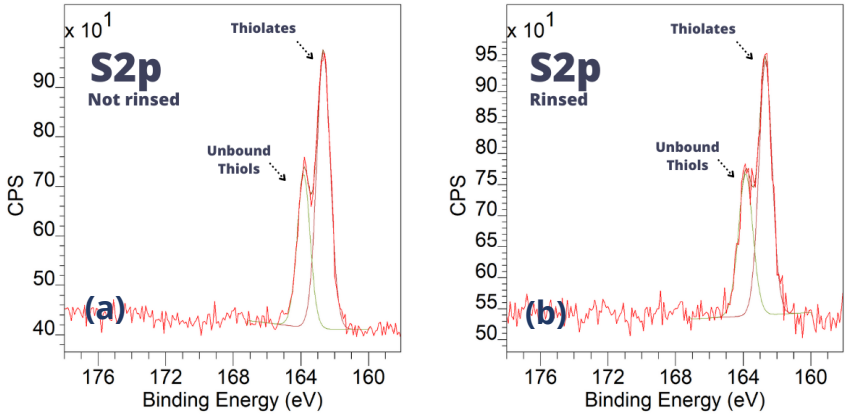

Figure 43: High-resolution XPS spectra of the S2p peak for copper submerged in an ethanolic 1-octanethiol (1mM) solution for 1 hour, both (a) not rinsed and (b) rinsed

Figure 43 shows the high-resolution spectra of the S2p peaks for both the not rinsed (a) and rinsed (b) sample that was submerged in the thiolic solution for one hour. Both spectra (a) and (b) look rather similar and have a large contribution at 162 eV (thiolates) and a smaller contribution at 163 eV (unbound thiols). The contribution of thiolates was calculated to be on average 62% for both samples. The ratios of the atomic concentrations will help to define the coverage of the sample and can be deduced from Figure 44.

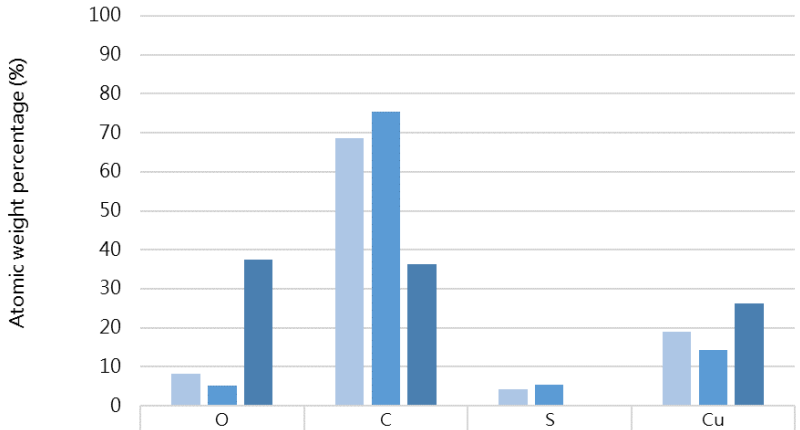

	O	C	S	Cu
Cu + 1-octanethiol (1mM) - Not rinsed	8	69	4	19
Cu + 1-octanethiol (1mM) - Rinsed	5	75	5	14
Bare copper	37	36	0	26

Figure 44: Atomic weight percentage of O, C, S and Cu for copper submerged in an ethanolic 1-octanethiol (1mM) solution for one hour (rinsed and not rinsed) compared to the bare substrate

As derived from Figure 44, the C/Cu ratio is equal to 3,6 which is higher than the C/Cu ratio for bare copper (1,4), which can be explained by the adhesion of thiol species. The S/C ratio is equal to 0,06 which is about half the S/C ratio of 1-octanethiol (0,13). This indicates that some contamination is still present on the sample, as not all carbon originates from the thiol molecule.

A good interaction between copper and thiols is thus observed, as confirmed by the C/Cu ratio, the S/C ratio that corresponds to the stoichiometric ratio and the high amount of thiolate species. The mechanism and bond strength behind this interaction should be further investigated using complementary techniques such as ToF-SIMS. In literature, the sulfur was said to interact best with the unsaturated copper atom (Cu_{cus} as indicated by Chiter et al.[57] and explained in section 3.2.4.).

5.3. How can the hybrid interaction be improved by changing the surface state of copper?

The final goal of this thesis is to investigate the effect that the chemical surface state of copper metal can have on the bond formation. This will be done by creating different copper oxide surfaces and comparing their interaction with thiolic solutions by investigating these samples using high-resolution XPS spectra. Before the submersion test can be performed, stable and well characterized copper oxides must be produced.

5.3.1. Production of copper oxides

The first challenge is to produce and characterize a controlled and homogeneous oxide on the copper surface. This was first done using uncontrolled heating, meaning that the sample was simply placed in a preheated oven and was thus heated up using a very steep temperature gradient, going from 25 °C to 350 °C in a couple of seconds. The cooling process was performed in a similar way. As can be seen in Figure 45 (b), this leads to a build-up of internal stresses between the oxides and a subsequent delamination between the oxides occurs. This effect was predicted by literature, as described in section 3.4. This sample is, of course, not suitable for proper adhesion.

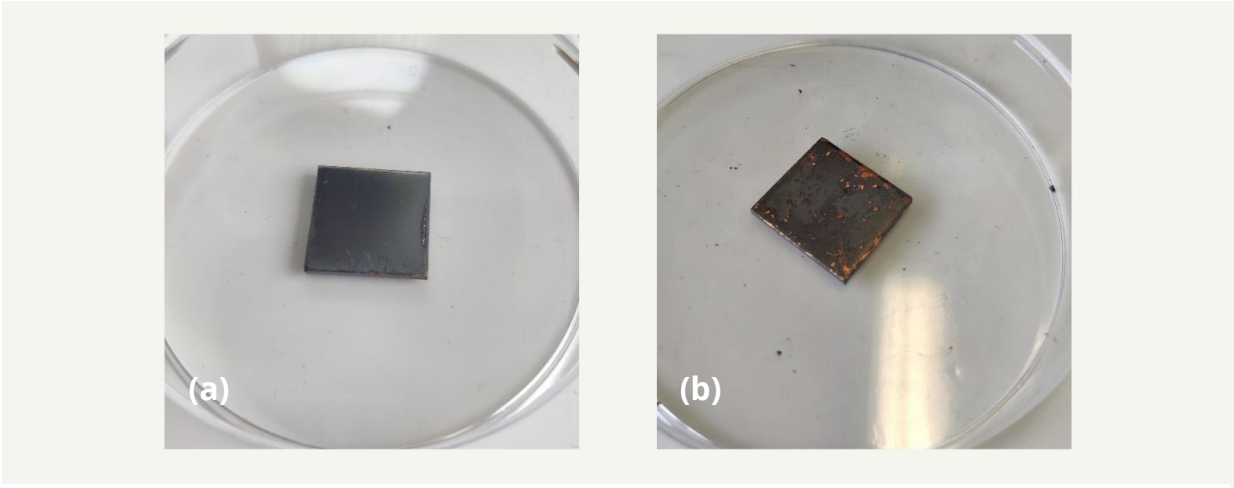

Figure 45: Copper produced using (a) controlled heating and cooling at 10 °C/min and (b) without controlled heating and cooling at 350 °C for 3h

In this sample the top layer appears grey, whereas the spots where the oxide peeled off appear red. After a controlled heating using a 10°C/min heating and cooling rate, as shown in Figure 45 (a), a smooth oxide layer is obtained. Both these samples were analyzed using high-resolution XPS spectra of the C1s, O1s, Cu2p and CuLMM peaks to investigate the nature of the top oxides layer. The recorded spectra for the partially delaminated sample are shown in Figure 46.

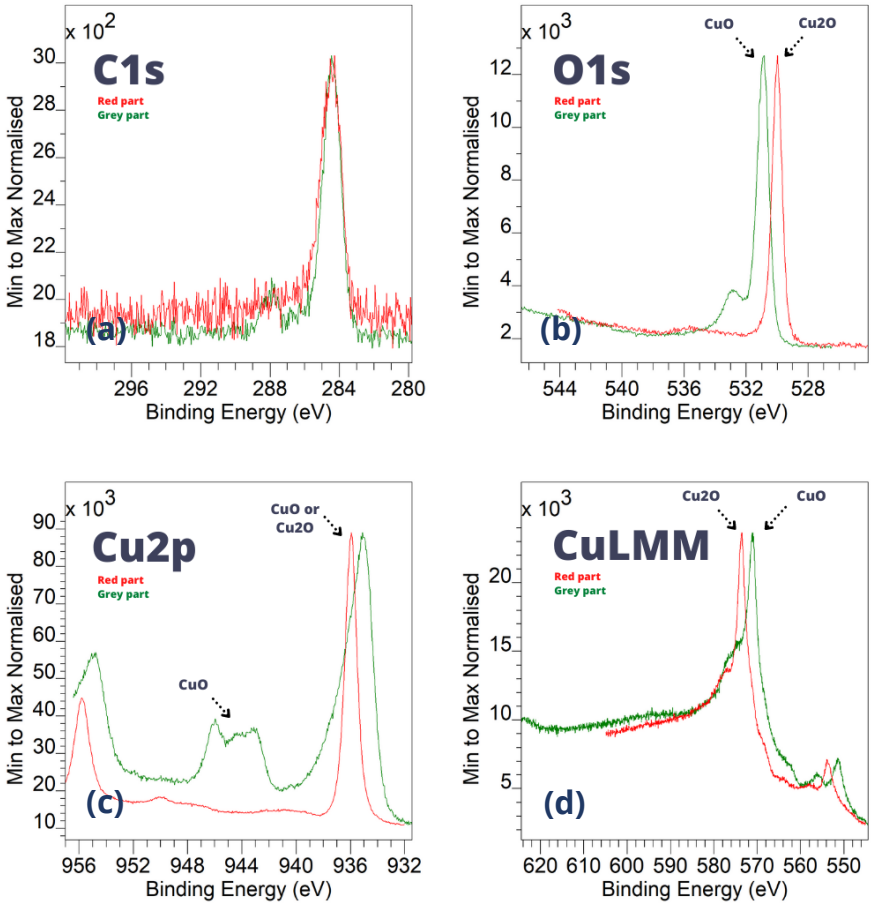

Figure 46: High-resolution XPS spectra of the (a) C1s peak, (b) O1s peak, (c) Cu2p peak and (d) CuLMM peak for the red part shown in red and the grey shown in green for copper heated to 350°C for 3h without controlled heating as shown in Figure 46 (b).

The C1s peak in Figure 46 (a) looks similar for both the red area and the grey are of the delaminated sample, meaning that they contain a similar surface contamination. The red O_{1s} peak in Figure 46 (b) shows a contribution around 531 eV which is typically identified as either Cu_2O, whereas the green peak has a contribution at higher binding energies, indicating the presence of CuO. The red Cu2p peak in Figure 46 (c) has only one contribution at 936 eV, which indicates the presence of Cu_2O, whereas the green spectrum clearly contains a sattelite peak at 942 eV which indicates the presence of CuO species. The red CuLMM spectrum in Figure 46 (d) indicates the presence of Cu_2O species at around 570 eV, whereas the green peak is found at somewhat lower binding energies, indicating the presence of CuO species. The grey area (illustrated by the green peaks) of the partially delaminated sample thus clearly contains more CuO, while the red area contains more Cu_2O.

To be able to perform submersion tests, the controlled heating experiment was repeated, now at two different temperatures (300 °C and 350 °C) to try and form a smooth CuO layer on the one hand and a Cu_2O layer as suggested by Choudhary et al.[37] Due to time limitations, the surface of these oxides were characterized using Raman spectroscopy, as reported in Figure 47.

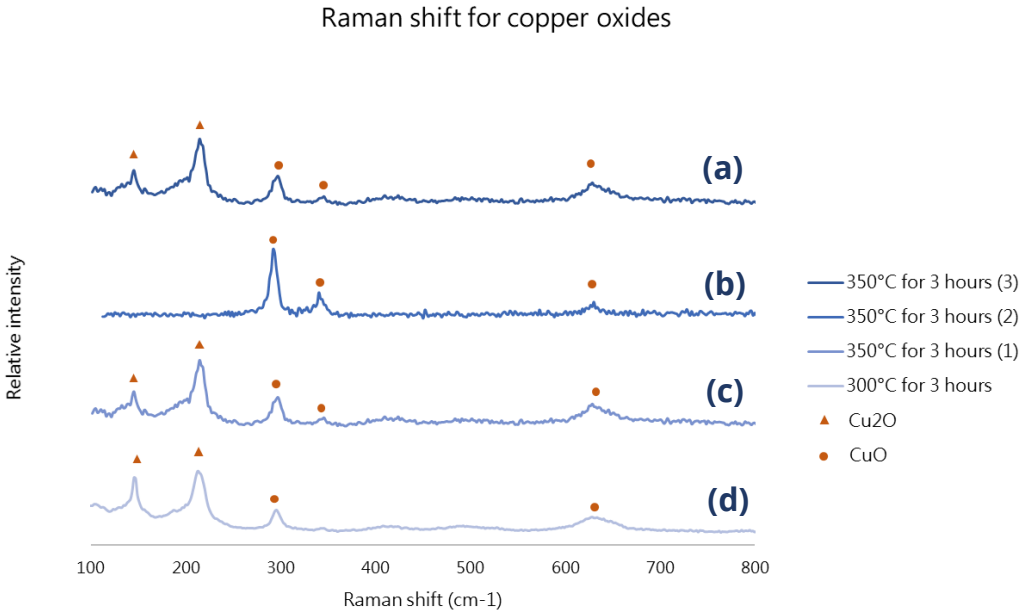

Figure 47: Raman spectrum for the copper oxides produced in a controlled oven during 3 hours using 10°C/min heating and cooling rates (a) at 350°C for a first spot, (b) at 350°C for a second spot, (c) at 350°C for a third spot and (d) at 300°C. The signifying Cu_2O peaks are highlighted using a ▲ and the CuO species are highlighted using a •.

Figure 47 reports the Raman spectrum for the copper samples that were heated at 300°C and 350°C using controlled heating. The peaks at 149 and 221 cm^{-1} illustrate the presence of Cu_2O, while the peaks at 298 cm^{-1}, 308 cm^{-1} and 602 cm^{-1} illustrate the presence of CuO.[103] Figure 47 (a), (b) and (c) show a mixture of both copper oxides and illustrate the inhomogeneity of the sample. Figure 47 (d) also shows a mixture of both copper species.

Raman measurements can, however, due to their depth resolution give a false idea of the composition of the top layer. XPS measurements, which are much more top sensitive, allowed to conclude that the grey color seen in Figure 46 (a) and (b) illustrates the presence of CuO. Since both the samples heated at 300°C and 350°C had a grey appearance, it can be concluded that their top surface consists of mainly CuO.

5.3.2. Submersion of copper oxides in thiolic solutions

To understand the effect of the copper oxides on the interaction with thiolic solutions, both the delaminating sample and the samples containing a smooth oxide layer were submerged in a 1-octanethiol (1mM ethanolic) solution. To evaluate the interaction with Cu_2O, the red parts of the delaminated sample (Figure 45 (b)) was analyzed as they contained mostly Cu_2O. To evaluate the interaction with CuO, the samples produced in the controlled oven were used, as they contained mostly CuO on the surface layer. As from now, these samples will be referred to as Cu_2O and CuO respectively. The samples were examined using the high-resolution XPS spectra of the C1s, O1s, Cu2p, CuLMM and S2p peak. The first four peaks are used to investigate the effect of the thiol on the oxide layer, while the S2p is decomposed into thiolate and unbound thiol contribution to evaluate the interactions. These peaks were also used to determine the atomic concentrations of the present elements, as well as the S/C ratio and the S/Cu ratio to investigate the relative amount of thiolate species present compared to the bare substrate.

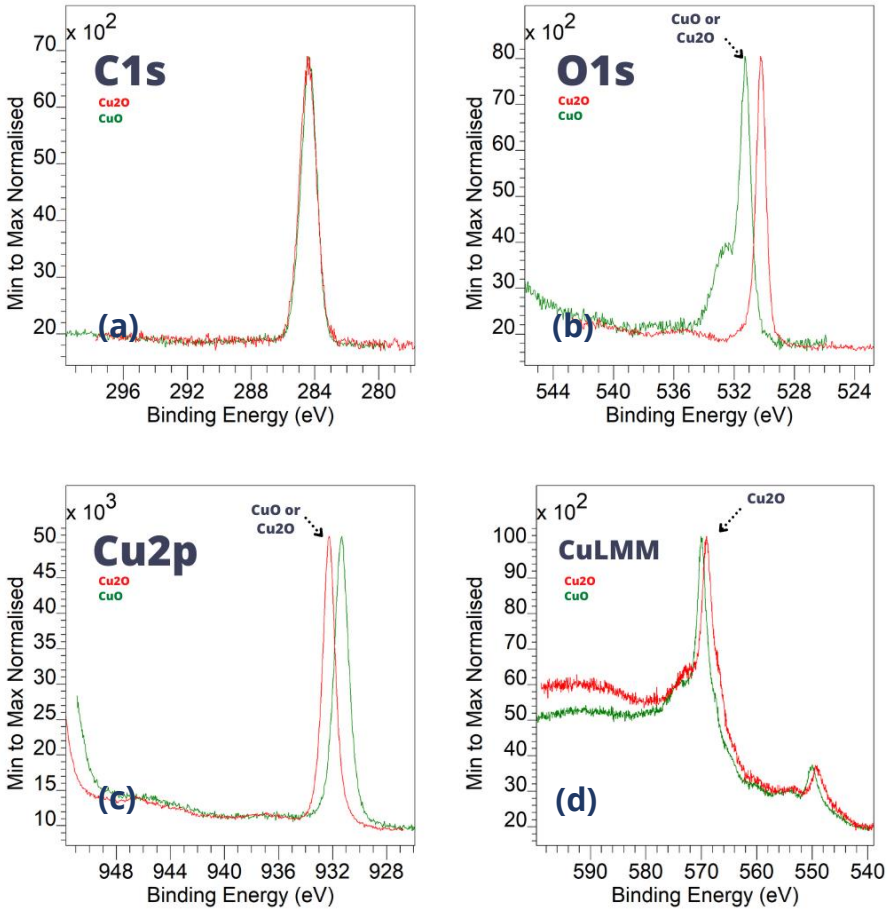

Figure 48: High-resolution XPS spectra of the (a) C1s peak, (b) O1s peak, (c) Cu2p peak and (d) CuLMM peak for Cu_2O (red) and CuO (green) submerged in 1-octanethiol for 1 hour.

The high-resolution spectra of the C1s (a), O1s (b), Cu2p (c) and CuLMM (d) peak are reported in Figure 48. The C1s peak (a) is similar for both spectra. The O1s peak (b) is similar to that observed before submersion, showing a peak at 532 eV for the green spectrum and 531 eV for the red spectrum, indicating a CuO layer for the green spectrum and a Cu_2O layer for the red spectrum.

The peaks are, however, rather close to one another, making it difficult to distinguish these species. The Cu2p peak (c) of the green spectrum lacks the typical CuO satellite, indicating its absence after submersion in thiols. The CuLMM (d) peak of the green spectrum at 570 eV compared to 569 eV before submersion, confirms that the CuO is transformed to Cu_2O after submersion. The red Cu2p (c) and CuLMM (d) peaks remained the same as before submersion, also indicating the presence of Cu_2O. To investigate bond formation, the S2p peak was decomposed as described in section 4.3.1.1. These peaks are reported in Figure 49.

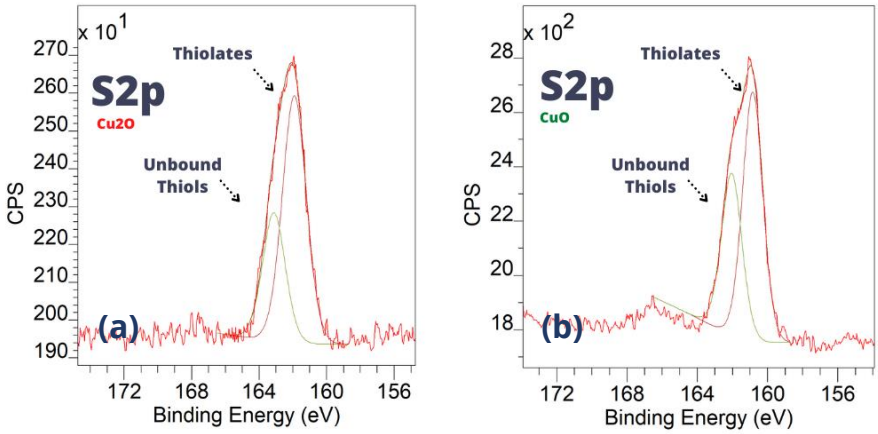

Figure 49: High-resolution XPS spectra of the S2p peaks for (a) Cu_2O and (b) CuO submerged in 1-octanethio for 1 hour. The peaks are decomposed as described in section 4.3.1.1. using a thiolate contribution at 162 eV and a contribution by the unbound thiols at 163 eV.

Figure 49 shows the peak fitting for both S2p peaks of the submersed Cu_2O (a) and CuO (b). The peaks look rather similar, with a slightly higher peak of unbound thiols (at 162 eV) for the CuO sample (b).

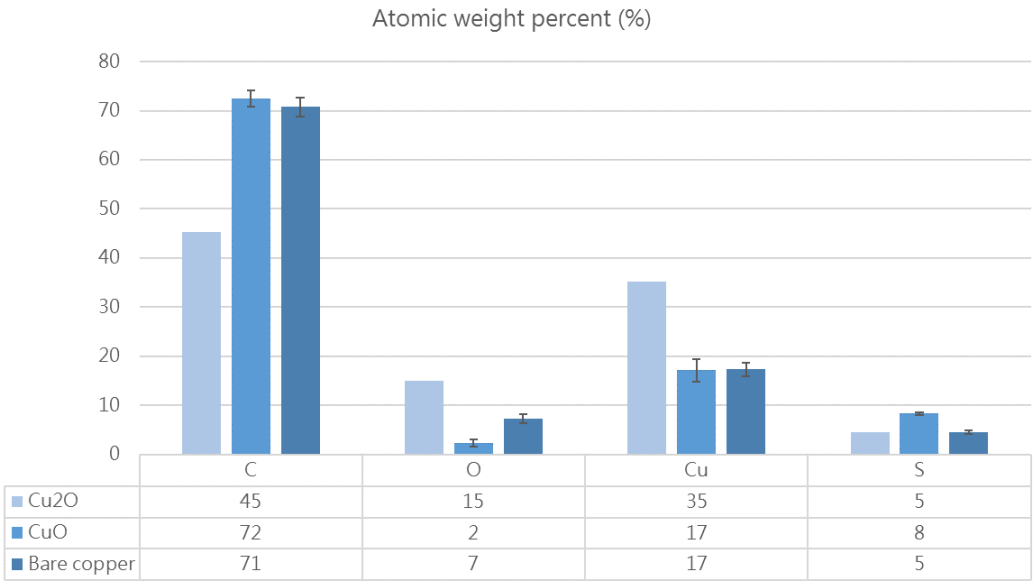

Figure 50: Atomic weight percent for the submersion of copper and different copper oxides in 1-octanethio (1mM) for 1 hour.

Figure 50 clearly indicates a difference in the atomic weight percentages of the different samples after submersion. The S/C ratio for both oxides is equal to 0,11, whereas that of bare copper is equal to 0,07. The S/C ratio is much closer to the stoichiometric ratio of 0,12 for the oxides than for the bare copper substrate. This illustrates the good adsorption of 1-octanethiol on the oxides. The Cu/S ratio is equal to 5 for the Cu_2O and 2,5 for the CuO, indicating a larger amount of thiols adsorbed for the CuO layer. The relative number of thiolates can give an idea on the number of interacting thiol species on the substrate. These numbers are compared for the Cu_2O, CuO and bare substrate submersion in Figure 51.

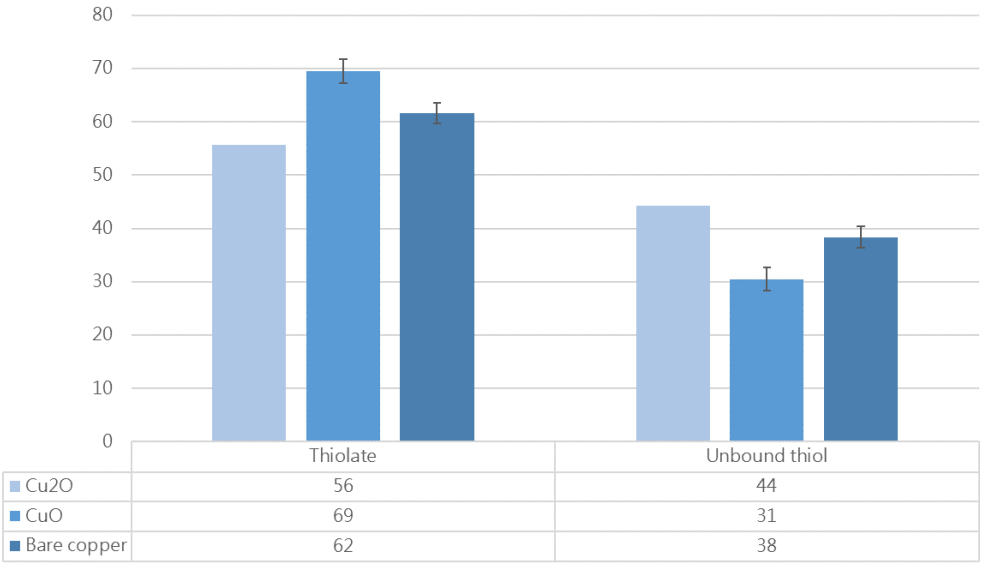

	Thiolate	Unbound thiol
Cu2O	56	44
CuO	69	31
Bare copper	62	38

Figure 51: Relative contributions of thiolates and unbound thiols for the submersion of copper and different copper oxides in 1-octanethiol (1mM) for 1 hour.

Figure 51 illustrates the relative amount of thiolate species on the sample. The number of thiolates is about 15% larger for the CuO layer compared to the Cu_2O layer, indicating a better interaction with this type of interface.

The improved interaction between thiol species and the CuO layer (compared to the bare substrate and the Cu_2O layer) and its transformation from Cu_2O to CuO are not easy to explain. In some way, the chemical composition of the surface influences the bond formation. To what extend and following what mechanism is to be investigated using complementary research techniques such as ToF-SIMs to evaluate the formed complexes or IR spectroscopy in a Kretschmann configuration to determine the evolution of this formation in time.

6. Discussion

XPS measurements showed that the gold and copper used Myanmar did not differ all too much from that provided by Goodfellow. The major difference is the amount of organic contamination due to rolling processes, deep into the material. The effect of this contamination on bond formation is another topic, which is out of the scope of this thesis. Gold can be assumed to be pure, while copper contains a complex native oxide layer consisting of $Cu(OH)_2$, CuO and Cu_2O respectively. The hydroxyl fraction of the copper from Goodfellow was substantial (21 %), higher than the hydroxyl fraction of the copper from Myanmar (11%).

The amines, as found in the used Huntsman glue and mimicked using DETA, show only poor interaction with the gold and a strong interaction with copper. The N/Au ratio (0,1) is much lower than the N/Cu (2,9) ratio, which illustrates the poor interaction with gold and the strong interaction with copper. The interaction between copper and amines turned out to be a Lewis-type and thus strong interaction. This was illustrated by combining the N1s peak decomposition with the findings from TOF-SIMS, which clearly showed an N2 contribution as well as the presence of copper-DETA complexes. The mechanism behind this bond formations is, however, not yet fully understood. By performing a submersion experiment with a higher concentration and comparing the rinsed samples to non-rinsed samples, one could postulate enhanced wet adhesion, as the rinsed case showed a higher N/C ratio and larger N1 component. More tests should be performed to truly understand the mechanism and the effect of the oxidation state of the surface.

An alternative for the adhesive that is currently used on the pagoda can thus be interesting, as it only interacts with copper, while the used gold seemed to be embedded and will delaminate after a certain amount of time. Even if the other factors, like temperature and a corrosive environment, play a major part in the delamination, a solution for this problem can be to improve the chemical interaction between the substrates and the adhesive.

Natural oils, as used in cultural heritage, were the inspiration for the use of succinic acid to investigate their possible use as an adhesive. A good interaction with copper and again a poor interaction with gold as seen in the XPS results by the a COO^{-}contribution of 3% for gold versus 8% for copper and the C/O ratio that approximated the stoichiometric ratio of the thiols for copper, but was much higher than that ratio for gold. Natural oils are, however, used to apply gold leaf and can endure for over 25 years or longer, as compared to five years for the gold of the pagoda.[4] The key aspect seems to be the thickness of the used gold plates. Due to minor defects in the gold leaf, it is possible that the glue migrates to the top of the gold layer and this way embeds the gold in a glued layer. Further investigations to the true mechanism behind this durability is required.

Thiols are described in literature as an interesting candidate for adhesion for both copper and gold.[60,61,72,73,77,78,80,81,102] XPS measurements showed that there is indeed a strong interaction with

copper and gold. For gold, however, a 24 hour submersion is required, as the self-assembly of the thiols on gold take time. This can indicate the importance of time for other bond formations, such as those with carboxylic acids, as well. Thiol based glues can therefore be a durable solution for the application of gold on cultural heritage.

As thiols are a very interesting candidate, it is also important to understand the effect of the surface state of copper on the bond formation, as it might improve or reduce the adhesion strength during in situ application. The production of stable copper hydroxides is very difficult and therefore also not as interesting for use on the pagoda. This in contrast with aluminium hydroxides, which are readily formed and were proven to improve the chemical bond formation. For copper, a homogeneous $Cu^{(2+)}$ oxide layer can be formed using controlled heating, at 10°C/min for heating and cooling. If the sample is heated in an uncontrolled way, internal stresses will cause delamination. XPS measurements showed an increased amount of thiolates compared to unbound thiols for the CuO layer, when comparing it to the bare copper and a layer that contains mainly Cu_2O. During submersion, the CuO was reduced to Cu_2O.

7. Conclusion

The delamination issue on the pagoda is not easy to solve as it is multifactorial and interdisciplinary. It brings together the word of cultural heritage and that of surface science in a way that they have never been brought together before. The problem must be subdivided into several categories and brought back together in the end, in order to be able to tell a comprehensive story and find an exhaustive solution. Therefore, this thesis used the delamination as an opportunity to investigate the effect of the surface state of metals on the chemical bond formation, and more specifically looked at the difference between a noble metal and a metal that readily forms a natural oxide layer. Model metals and molecules were used to mimic the specific case on the Shwedagon Pagoda.

Literature provides some first insights into this issue, but many questions remain unanswered. How does chemical bond formation between gold and organic material translate into an adhesive layer on molecular scale? What are the mechanisms behind chemical bond formation between copper and organic materials and how are they influenced by the oxidation state of the metal? All the while considering that it is difficult to characterize the surface state in the first place, due to the proximity of peaks in XPS spectra and the possible change in binding energy due to a wide variety of factors.

This research clearly showed a difference between the interactions between organic material and a noble metal (gold) compared to a metal that contains a native oxide layer (copper). The copper interacts well with all model molecules, whereas gold shows less or no interaction. This can of course be explained due to the thermodynamic stability of the gold metal, which requires a good oxidizing agent and ligand to be able to interact as shown in the literature study. An interesting conclusion from the results on thiols, however, is the importance of the time required for self-

assembly. This shows how time can be a governing parameter for interaction with gold. A noble metal is not by definition unable to interact with organic species, it just requires the right conditions to be met. The importance of the chemical state of the substrate is confirmed by the difference in interactions between different copper oxides and the bare substrate.

A second conclusion is that the gold on the pagoda specifically seems to be encapsulated in a glue layer with which there is only little chemical interaction. If the top glue layer were to get damaged throughout time, there are only few forces that keep the gold adhered to the underlying glue layer. If the thick gold plates are to be adhered in a durable manner, a strong chemical interaction with the organic material needs to be ensured. The results showed that this is not the case for the amine groups that are present in the glue that was currently used.

A final conclusion is that, in order to understand the true mechanism behind the chemical bond formation and the obtained type of interaction between metals and organic species, XPS results need to be extended using a complementary technique that allows to evaluate the formation of specific complexes (such as ToF-SIMS) and the effect of time (such as IR in a Kretschmann configuration).

8. Future research

Since this work is a preliminary research regarding the delamination of the gold on the Shwedagon Pagoda, many future characterizations are required to truly understand and solve the issue. This research does, however, highlight some major points of interest and allows future researchers to work more focused on some topics. In order to draw further conclusions, some tests should be performed again, in order to validate their scientific accuracy.

First of all, it is interesting to learn more about the current use of natural oils and to discover the true mechanism behind the durability of gold leaf on cultural heritage. Therefore, a microscopic evaluation of the natural oils in time can be performed to verify the 'embedding' hypothesis. This can be done using optical microscopy and standard adhesion tests, to evaluate the effect of the thickness of the gold plate on the adhesion strength.

Secondly, the use of thiols can further be explored, to see if a connection can be made between the thiol-based adhesion layer and actual glues. The effect of the oxidation state of copper can be verified even more and supplementary tests on gold can be performed to evaluate the effect of time. The effect of a roughening of the surface can also be evaluated using XPS, as it might increase the surface available for chemical bond formation. It must be evaluated whether this is the reason for better adhesion on the CuO layer, by varying the roughness of the substrate. Besides this, the effect of temperature, humidity and a corrosive environment on these bonds can be evaluated in a climate chamber.

It is also important to evaluate the delamination of the oxide layer on copper, as it was shown to occur during fast heating and cooling. This can be evaluated using thermal cycles and verified using XPS or Raman spectroscopy.

Once the mechanisms behind the chemical bond formation are fully understood, this information can be used as a background to evaluate the true adhesion strength using thiol-based glues and standard adhesion testing. Possible causes for stresses on the interfacial bonds and thus delamination should be verified. These stresses can be caused by a great deal of factors, which can in turn by categorized into three main sections; insufficient inherent adhesion properties, thermal stresses between the organic material and the metal or external factors such as water and salts that can in turn cause corrosion. These three categories are represented in Figure 52. This thesis of course already laid out a path to analyze the first factor.

The sun on the roof allows for temperatures up to 80°C. Because of this large temperature range, it is possible that the used glue goes through its glass transition. This means that the expansion coefficient of the glue might change significantly, causing large stresses at the interface as the expansion coefficients of metals and polymers can differ up to two orders of magnitude.[104] The damage caused by these stresses might increase if the presence of saline water, due to the proximity of the coast, produces corrosion products.[105,106] These effects must be overcome by the interfacial forces that exist between the copper and the organic layer as well as the gold and the organic layer. Defining the origin of the stresses on the interfacial bonds is thus very broad and interdisciplinary topic, which calls for a need to subdivide the issue into smaller sections and investigate each issue separately. After these investigations, all information should be brought together to solve the delamination issue in a comprehensive manner.

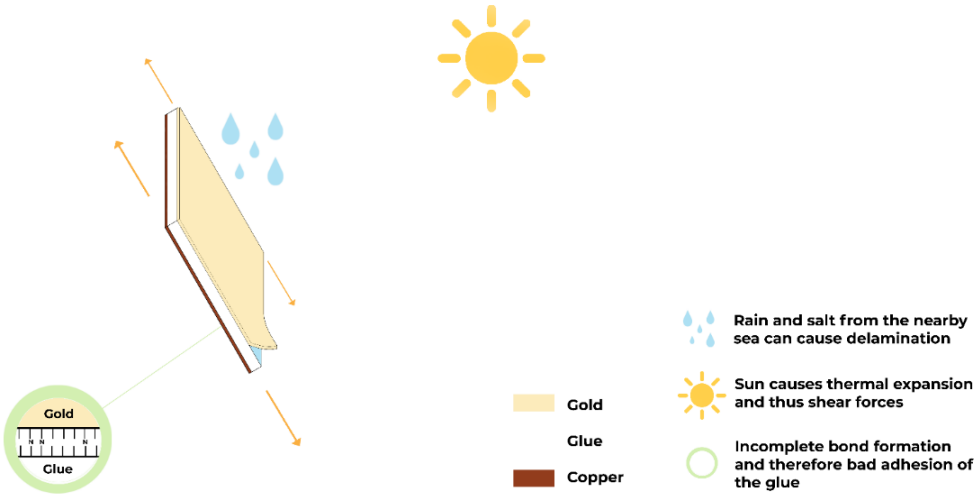

Figure 52: Schematical representation of possible causes of delamination of the gold-glue-copper system.

Finally, in situ measurements using IR spectroscopy can be performed, to truly understand the whole process ranging from the formation of the bonds, possible mechanism that enhance adhesion and finally to identify the failure of the system.

9. References

1. What you should know before you visit the Shwedagon Pagoda. Published online 2017
2. Ko A. Application of Shwedagon Pagoda as UNESCO world heritage. Published online 2018
3. Terryn H, Hauffman T, Vermeersch L. Private conversations with researchers from Yangun University, prof. dr. ir. Herman Terryn and prof. dr. ir. Tom Hauffman. (2020).
4. Terryn H, Hauffman T, Vermeersch L, Cattersel V, Storme P. Private conversation with researchers from the University of Antwerp (Research group ARCHES), prof. dr. ir. Herman Terryn and prof. dr. ir. Tom Hauffman. (2021).
5. de Wit JHW, van der Weijde DH, Ferrari G. Organic coatings. *Corros Mech Theory Pract Third Ed.*, 863-906. (2011).
6. Packham DE. *Handbook of Adhesion*. Vol 1. (John Wiley & Sons, 2005).
7. Critchlow G. Theory of adhesion. *Handbook of Adhesion Technology*. Vol 2. (Springer, 2011)
8. Ebnesajjad S. Theories of Adhesion. In: *Surface Treatment of Materials for Adhesive Bonding*. 77-92 (Elsevier, 2011)
9. Watts JF. The Interfacial Chemistry of Adhesion. Novel Routes to the Holy Grail? In: *Adhesion: Current Research and Applications*. (Wiley-VCH, 2005).
10. Moulijn JA. Bonding and elementary steps in catalysis. *Stud Surf Sci Catal*. 89-158 (1993).
11. Marcus P, Protopopoff É, Maurice V. Surface chemistry and passivation of metals and alloys. *Mech - Microstruct - Corros Coupling Concepts, Exp Model Cases*. (2019).
12. Rodriguez JA, Chaturvedi S, Kuhn M. A comparison of the reaction of S2 with metallic copper, Cu2O and Cu/ZnO: Electronic properties and reactivity of copper. *Surf Sci*. **415,** 1065-1073 (1998).
13. Escaig B. Binding metals to polymers. A short review of basic physical mechanisms. *J Phys*. **3**, 753-761 (1993).
14. Ochoa-Putman C, Vaidya UK. Mechanisms of interfacial adhesion in metal-polymer composites - Effect of chemical treatment. *Compos Part A Appl Sci Manuf*. **42,** 906-915 (2011)
15. Rance D Thermodynamic approach to adhesion problems. *Brewis D Ind Adhes Probl*. Published online 1985.
16. Brewis D Surface analysis and pretreatment of plastics and metals. **4,** (1982).
17. Malpass BW, Packham DE, Bright K. A study of the adhesion of polyethylene to porous alumina films using the scanning electron microscope. *J Appl Polym Sci*. **18**, 3249-3258 (1974).
18. Abrahami ST, de Kok JMM, Gudla VC, Ambat R, Terryn H, Mol JMC. Interface strength and degradation of adhesively bonded porous aluminum oxides. *npj Mater Degrad*. (2017).
19. Critchlow G (Loughborough U. *Handbook of Adhesion Technology*. (2011).
20. Wielant J, Hauffman T, Blajiev O, Hausbrand R, Terryn H. Influence of the iron oxide acid-base properties on the chemisorption of model epoxy compounds studied by XPS. *J Phys Chem C*. **35,** 13177-13184 (2007).
21. Taheri P, Hauffman T, Mol JMC, et al. Molecular interactions of electroadsorbed carboxylic acid and succinic anhydride monomers on zinc surfaces. *J Phys Chem C*. **34**, 17054-17067 (2011).
22. Alexander MR, Thompson GE, Beamson G. Characterization of the oxide/hydroxide surface of

aluminum using X-ray photoelectron spectroscopy: A procedure for curve fitting the O 1s core level. *Surf Interface Anal*. **29**, 468-477 (2000).

23. Oh Y-J, Park G-S, Chung C-H. Planarization of Copper Layer for Damascene Interconnection by Electrochemical Polishing in Alkali-Based Solution. *J Electrochem Soc*. **153,** 617 (2017).
24. Strehblow H -H, Speckmann H -D. Corrosion and layer formation of passive copper in alkaline solutions. *Mater Corros*. **35**, 512-519 (1984).
25. Noli F, Misaelides P, Hatzidimitriou A, Pavlidou E, Kokkoris M. Investigation of artificially produced and natural copper patina layers. *J Mater Chem*. **13**, 114-120 (2003)
26. Platzman I, Brener R, Haick H, Tannenbaum R. Oxidation of polycrystalline copper thin films at ambient conditions. *J Phys Chem C*. **112**, 1101-1108 (2008).
27. Chavez KL, Hess DW. A Novel Method of Etching Copper Oxide Using Acetic Acid A Novel Method of Etching Copper Oxide Using Acetic Acid. (2014).
28. Zhou JC, Soto CM, Chen M, et al. Biotemplating rod-like viruses for the synthesis of copper nanorods and nanowires. Published online 2012
29. Sobol PE, Chastain J. Handbook of X-ray Photoelectron Spectroscopy. Published online 1992.
30. Moretti G, Palma A, Paparazzo E, Satta M. Auger parameter and Wagner plot studies of small copper clusters. *Surf Sci*. **646**, 298-305 (2016).
31. Massey R, Zee A, Gmbh AD. Use of non etching adhesion promotors in advanced PCB applications. *Structure* (2010).
32. Lin Y Sen, Liu HM. A study on the adhesion performance of copper to polyimide for microelectronic packaging-flex substrates. *Proc 4th Int Symp Electron Mater Packag EMAP.* 182-187 (2002).
33. Granado L, Kempa S, Gregoriades LJ, et al. Improvements of the Epoxy–Copper Adhesion for Microelectronic Applications. *ACS Appl Electron Mater*. 1498-1505 (2019).
34. Fulazzaky MA, Fulazzaky M, Sumeru K. Evaluation of coating rate and adhesive force for copper deposition on the surface of polypropylene. *J Adhes Sci Technol*. **33**, 1438-1452 (2019).
35. Zheng JY, Van TK, Pawar AU, Kim CW, Kang YS. One-step transformation of Cu to Cu2O in alkaline solution. *RSC Adv*. **4**, 18616-18620 (2014).
36. Hollmark HM, Keech PG, Vegelius JR, Werme L, Duda LC. X-ray absorption spectroscopy of electrochemically oxidized Cu exposed to Na2S. *Corros Sci*. **54,** 85-89 (2012).
37. Choudhary S, Sarma JVN, Pande S, et al. Oxidation mechanism of thin Cu films: A gateway towards the formation of single oxide phase. *AIP Adv.* **8**, (2018).
38. Gurav K V., Patil UM, Shin SW, et al. Room temperature chemical synthesis of Cu(OH)2 thin films for supercapacitor application. *J Alloys Compd*. **57**, 27-31 (2013).
39. Nothdurft P, Riess G, Kern W. Copper/epoxy joints in printed circuit boards: Manufacturing and interfacial failure mechanisms. *Materials (Basel)*. (2019).
40. Lebbai M, Szeto WK, Kim JK. Optimization of black oxide coating thickness as adhesion promoter for copper substrate. *Int Symp Electron Mater Packag EMAP*. **32**, 206-213 (2000).
41. Evans JR, Packham DE. Adhesion of Polyethylene to Copper: Importance of Substrate Topography. *J Adhes*. **10**, 39-47 (1979).
42. Bright K, Malpass BW, Packham DE. Adhesion of Polyethylene to Metals. *Nature*. **223** (1969).
43. Evans JRG, Packham DE. Adhesion of Polyethylene to Copper: Reactions Between Copper Oxides and the Polymer. *J Adhes*. **9**, 267-277 (1978).
44. Hoque E, Derose JA, Houriet R, Hoffmann P, Mathieu HJ. Stable perfluorosilane self-assembled monolayers on copper oxide surfaces: Evidence of siloxy-copper bond formation. *Chem Mater*. **19**, 798-804 (2007).
45. Deflorian F, Rossi S, Fedrizzi L, Fedel M. Integrated electrochemical approach for the investigation of silane pre-treatments for painting copper. *Prog Org Coatings*. **63**, 338-344 (2008).

46. Honkanen M, Hoikkanen M, Vippola M, Vuorinen J, Lepistö T. Aminofunctional silane layers for improved copper-polymer interface adhesion. *J Mater Sci*. **46**, 6618-6626 (2011).
47. Karthik N, Sethuraman MG. Surface protection of copper by allyl thiourea and hybrid sol-gel coatings. *Prog Org Coatings*. **90**, 380-389 (2016).
48. Peng S, Zhao W, Li H, Zeng Z, Xue Q, Wu X. The enhancement of benzotriazole on epoxy functionalized silica sol-gel coating for copper protection. *Appl Surf Sci*. **276**, 284-290 (2013).
49. Allam NK, Hegazy HS, Ashour EA. Adsorption–Desorption Kinetics of Benzotriazole on Cathodically Polarized Copper. *J Electrochem Soc*. **157**, (2010).
50. Ding J, Chen C, Xue G. The dynamic mechanical analysis of epoxy–copper powder composites using azole compounds as coupling agents. *J Appl Polym Sci*. **42**, 1459-1464 (1991).
51. Antonijević MM, Milić SM, Petrović MB. Films formed on copper surface in chloride media in the presence of azoles. *Corros Sci*. **51,** 1228-1237 (2009).
52. Patil S, Sainkar SR, Patil PP. Poly(o-anisidine) coatings on copper: Synthesis, characterization and evaluation of corrosion protection performance. *Appl Surf Sci*. **225**, 204-216 (2004).
53. Brusic V, Angelopoulos M, Graham T. Use of polyaniline and its derivatives in corrosion protection of copper and silver. *Annu Tech Conf - ANTEC, Conf Proc*. **2**, 1397-1405 (1995).
54. Wu, X., Wiame, F., Maurice, V. et al. Molecular scale insights into interaction mechanisms between organic inhibitor film and copper. *npj Mater Degrad* **5**, 22 (2021)
55. Vernack E, Costa D, Tingaut P, Marcus P. DFT studies of 2-mercaptobenzothiazole and 2-mercaptobenzimidazole as corrosion inhibitors for copper. *Corros Sci*. **174**, 108840 (2020).
56. Chiter F, Costa D, Maurice V, Marcus P. Adsorption of 2-mercaptobenzimidazole Corrosion Inhibitor on Copper: DFT Study on Model Oxidized Interfaces. *J Electrochem Soc*. **167**, 161506 (2020)
57. Chiter F, Costa D, Maurice V, Marcus P. DFT investigation of 2-mercaptobenzothiazole adsorption on model oxidized copper surfaces and relationship with corrosion inhibition. *Appl Surf Sci*. **537**, 147802 (2021).
58. Chadwick D, Hashemi T. Electron spectroscopy of corrosion inhibitors: Surface films formed by 2-mercaptobenzothiazole and 2-mercaptobenzimidazole on copper. *Surf Sci*. **89**, 649-659 (1979).
59. Peng HE. Thiol Material Selection for Better Adhesion and reliability for copper/epoxy interface. [graduate thesis] Hong Kong, China: Hong Kong University of Science and technology (2011).
60. Wong CKY, Yuen MMF, Xu B. Thiol-based self-assembly nanostructures in promoting interfacial adhesion for copper-epoxy joint. *Appl Phys Lett*. **94**, 9-22 (2014).
61. Wang Y, Im J, Soares JW, Steeves DM, Whitten JE. Thiol Adsorption on and Reduction of Copper Oxide Particles and Surfaces. *Langmuir*. 32, 848-3857 (2016).
62. Crispin X, Bureau C, Geskin VM, Lazzaroni R, Salaneck WR, Brédas JL. Chemisorption of acrylonitrile on the Cu(100) surface: A local density functional study. *J Chem Phys*. **111**, 3237-3251 (1999).
63. Darque-Ceretti E, Felder E, Aucouturier M. Gilding of cultural heritage artefacts: An elaborated technology. *Surf Eng*. **29**, 146-152 (2013).
64. Oddy A. Gilding of Metals in the Old World. *In: Metal Plating and patination*: La Niece: Butterworth-Heinemann Ltd; (1993).
65. Mortier T. An Experimental Study on the Preparation of Gold Nanoparticles and Their Properties. [graduate thesis] Leuven, Belgium: Catholic University of Leuven (2006).
66. Franck J. The Nobel Prize and Aqua Regia. https://libretexts.org/ Pubkished online 2020.
67. Laguna A. Modern Supramolecular Gold Chemistry: Gold-Metal Interactions and Applications (Wiley & Sons, 2009).
68. Pyykkö P. Theoretical chemistry of gold. III. *Chem Soc Rev*. **37**, 1967-1997 (2008).
69. Pyykkö P. Theoretical chemistry of gold. *Angew Chemie - Int Ed*. **43**, 4412-4456 (2004).
70. Liu HT, Xiong XG, Diem Dau P, et al. Probing the nature of gold-carbon bonding in gold-alkynyl

complexes. *Nat Commun*. **4** (2013).
71. Hashmi ASK. Gold-Catalyzed Organic Reactions. 3180-3211. Published online 2007.
72. Urcuyo R, Cortés E, Rubert AA, et al. Aromatic and aliphatic thiol self-assembled monolayers on Au: Anchoring and delivering copper species. *J Phys Chem C*. **115**, 24707-24717 (2011).
73. Caipa Campos MA, Trilling AK, Yang M, et al. Self-assembled functional organic monolayers on oxide-free copper. *Langmuir*. **27**, 8126-8133 (2011).
74. Paik WK, Han S, Shin W, Kim Y. Adsorption of carboxylic acids on gold by anodic reaction. *Langmuir*. **19**, 4211-4216 (2003).
75. Rodriguez JA, Dvorak J, Jirsak T, et al. Coverage effects and the nature of the metal-sulfur bond in S/Au(111): High-resolution photoemission and density-functional studies. *J Am Chem Soc*. **125**, 276-285 (2003).
76. O'Dwyer C, Gay G, Viaris De Lesegno B, Weiner J. The nature of alkanethiol self-assembled monolayer adsorption on sputtered gold substrates. *Langmuir*. **20**, 8172-8182 (2004).
77. Fies WA, Dugger JW, Dick JE, et al. Direct Measurement of Water Permeation in Submerged Alkyl Thiol Self-Assembled Monolayers on Gold Surfaces Revealed by Neutron Reflectometry. *Langmuir*. Published online 2019.
78. Pensa E, Vericat C, Grumelli D, et al. New insight into the electrochemical desorption of alkanethiol SAMs on gold. *Phys Chem Chem Phys*. **14**, 12355-12367 (2012).
79. Frey BL, Corn RM. Covalent Attachment and Derivatization of Poly(L-lysine) Monolayers on Gold Surfaces As Characterized by Polarization-Modulation FT-IR Spectroscopy. *Anal Chem*. **68**, 3187-3193 (1996).
80. Bourg MC, Badia A, Bruce Lennox R. Gold-sulfur bonding in 2D and 3D self-assembled monolayers: XPS characterization. *J Phys Chem B*. **104**, 6562-6567 (2000).
81. Azzam W. Self-Assembled Monolayers on Gold Made from Organothiols Containing an Oligophenyl-Backbone. 164. Published online 2003.
82. Barysz M, Pyykkö P. Strong chemical bonds to gold. High level correlated relativistic results for diatomic AuBe + , AuC + , AuMg + , and AuSi +. *Chem Phys Lett*. **285**, 398-403 (1998).
83. Partyka D V., Updegraff JB, Zeller M, Hunter AD, Gray TG. Carbon-gold bond formation through [3 + 2] cycloaddition reactions of gold(I) azides and terminal alkynes. *Organometallics*. **26**, 183-186 (2007).
84. Antušek A, Blaško M, Urban M, et al. Density functional theory modeling of C-Au chemical bond formation in gold implanted polyethylene. *Phys Chem Chem Phys*. **19**, 28897-28906 (2017).
85. Leopold MC, Black JA, Bowden EF. Influence of gold topography on carboxylic acid terminated self-assembled monolayers. *Langmuir*. **18**, 978-980 (2002).
86. González-Liste PJ, García-Garrido SE, Cadierno V. Gold(i)-catalyzed addition of carboxylic acids to internal alkynes in aqueous medium. *Org Biomol Chem*. **15**, 1670-1679 (2017).
87. Baker TA, Liu X, Friend CM. The mystery of gold's chemical activity: Local bonding, morphology and reactivity of atomic oxygen. *Phys Chem Chem Phys*. **13**, 34-46 (2011).
88. Szakálos P, Hultquist G, Wikmark G. Corrosion of copper by water. *Electrochem Solid-State Lett*. **10**, 63-67 (2007).
89. Cho K, Cho EC. Effect of the microstructure of copper oxide on the adhesion behavior of epoxy/copper leadframe joints. *J Adhes Sci Technol*. **14**, 1333-1353 (2000).
90. Jackson ML. Copper/Epoxy Adhesive Performance and Durability (1999).
91. King DE. Oxidation of gold by ultraviolet light and ozone at 25 °C. *J Vac Sci Technol A Vacuum, Surfaces, Film*. **13**, 1247-1253 (1995).
92. Taheri P, Wielant J, Hauffman T, et al. A comparison of the interfacial bonding properties of carboxylic acid functional groups on zinc and iron substrates. *Electrochim Acta*. **56**, 1904-1911 (2011).
93. Abrahami ST, Hauffman T, De Kok JMM, Mol JMC, Terryn H. XPS Analysis of the Surface Chemistry and

Interfacial Bonding of Barrier-Type Cr(VI)-Free Anodic Oxides. *J Phys Chem C*. **119**, 19967-19975 (2015).

94. Pletincx, S., Fockaert, L.L.I., Mol, J.M.C. et al. Probing the formation and degradation of chemical interactions from model molecule/metal oxide to buried polymer/metal oxide interfaces. *npj Mater Degrad* **3**, 23 (2019).
95. Hauffman T, Blajiev O, Snauwaert J, Haesendonck C Van, Hubin A, Terryn H. Study of the self-assembling of n-octylphosphonic acid layers on aluminum oxide. *Langmuir*. **24**, 13450-13456 (2008).
96. Yeh JJ, Lindau I. Atomic subshell photoionization cross sections and asymmetry parameters: 1 ≤ Z ≤ 103. *At Data Nucl Data Tables*. **32**, 1-155 (1985).
97. Powell CJ, Jablonski A. NIST Electron Inelastic-Mean-Free-Path Database. Published online 2000)
98. Baer DR, Engelhard MH, Lea AS, et al. Comparison of the sputter rates of oxide films relative to the sputter rate of SiO2. *J Vac Sci Technol A Vacuum, Surfaces, Film*. **28**, 1060-1072 (2010).
99. Chan HYH, Takoudis CG, Weaver MJ. Oxide film formation and oxygen adsorption on copper in aqueous media as probed by surface-enhanced Raman spectroscopy. *J Phys Chem B*. **103**, 357-365 (1999).
100. Shields WR, Murphy TJ, Garner EL. Absolute isotopic abundance ratio and the atomic weight of a reference sample of copper. *J Res Natl Bur Stand Sect A Phys Chem*. **68**, 589 (1964).
101. Pletincx S, Trotochaud L, Fockaert LL, et al. In situ characterization of the initial effect of water on molecular interactions at the interface of organic/inorganic hybrid systems. *Sci Rep*. 3-10 (2017).
102. Pensa E, Cortés E, Corthey G, et al. The chemistry of the sulfur-gold interface: In search of a unified model. *Acc Chem Res*. **45**, 1183-1192 (2012).
103. Purusottam-Reddy B, Sivajee-Ganesh K, Jayanth-Babu K, Hussain OM, Julien CM. Microstructure and supercapacitive properties of rf-sputtered copper oxide thin films: influence of O2/Ar ratio. *Ionics (Kiel)*. **21**, 2319-2328 (2015).
104. Humfeld GR, Dillard DA. Residual stress development in adhesive joints subjected to thermal cycling. *J Adhes*. **65**, 277-306 (1998).
105. Rahmanto W, Gunawan, Nuryanto R. Corrosion Rate of Copper and Iron in Seawater Based on Resistance Measurement. *J Coast Dev.* **5**, 1410-5217 (2002).
106. Kook SY, Dauskardt RH. Moisture-assisted subcritical debonding of a polymer/metal interface. *J Appl Phys*. **91**, 1293-1303 (2002).

10. Annex

10.1. Peak decompositions of the O1s and C1s peaks for the model copper

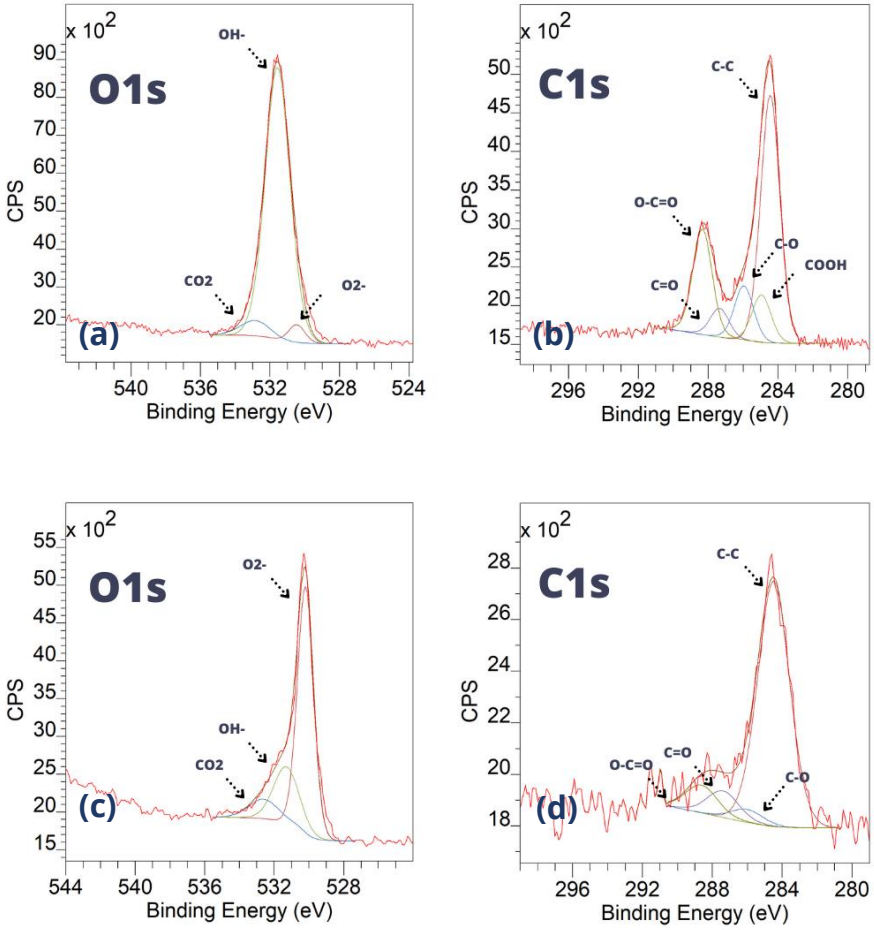

Figure 53: High-resolution XPS spectra of the (a) O1s peak for before sputtering, (b) C1s peak before sputtering, (c) O1s peak after sputtering and (d) C1s peak after sputtering. The decomposition procedure is given in section 4.3.1.1.

Table 11: Full width at half maximum (FWHM) for the peaks in Figure 53

Before/After sputtering	Peak	FWHM
Before sputtering	C1s contributions	1,28

After sputtering	C1s contributions	2,14

10.2. Peak decompositions of the O1s and C1s peaks for the copper from Myanmar

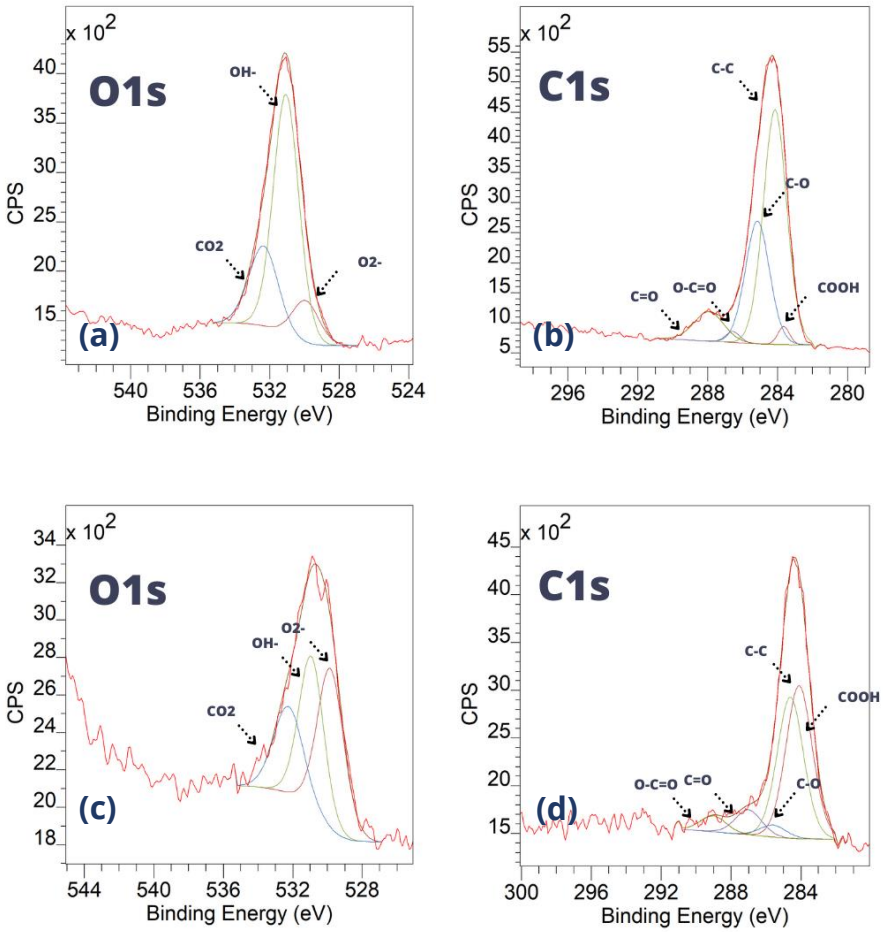

Figure 54: High-resolution XPS spectra of the (a) O1s peak for before sputtering, (b) C1s peak before sputtering, (c) O1s peak after sputtering and (d) C1s peak after sputtering. The decomposition procedure is given in section 4.3.1.1.

Table 12: Full width at half maximum (FWHM) for the peaks in Figure 54

Before/After sputtering	Peak	FWHM
Before sputtering	C1s contributions	1,28
After sputtering	C1s contributions	2,14

10.3. XPS measurements of submersion of copper in thiolic solution for 24h

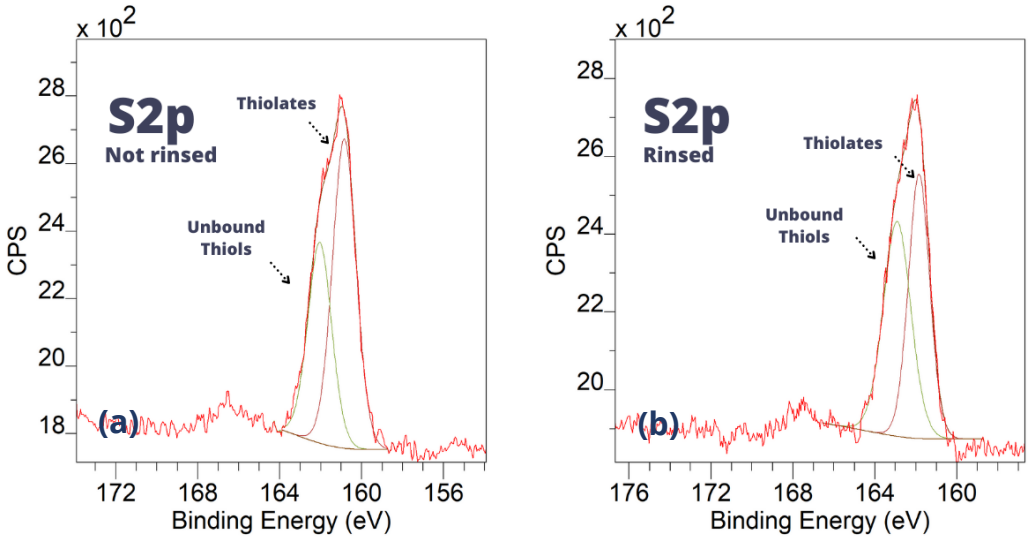

Figure 55: XPS High-resolution XPS spectra of the S2p peak for copper submerged in an ethanolic 1-octanethiol (1mM) solution for 24 hours, both (a) not rinsed and (b) rinsed

The results obtained for this sample were similar to the submersion for 1 hour.